Lipid droplets form a network interconnected by the endoplasmic reticulum through which they equilibrate their proteins

Stéphanie Cottier and Roger Schneiter*

Department of Biology, University of Fribourg, Chemin du Musée 10, 1700 Fribourg, Switzerland

Key words: Lipid droplets, endoplasmic reticulum, *Saccharomyces cerevisiae*, protein targeting, mating, membrane fusion, seipin, triacylglycerols, steryl esters

*Corresponding author: Roger Schneiter, Division of Biochemistry, Department of Biology, University of Fribourg, Chemin du Musée 10, 1700 Fribourg, Switzerland, Phone +41 26 300 8654, Email: roger.schneiter@unifr.ch

Abstract

Lipid droplets (LDs) are globular intracellular structures dedicated to the storage of neutral lipids. They are closely associated with the endoplasmic reticulum (ER) and are delineated by a monolayer of phospholipids that is continuous with the cytoplasmic leaflet of the ER membrane. LDs contain a specific set of proteins, but how these proteins are targeted to the LD surface is not fully understood. Here we devised a yeast mating-based microscopic readout to monitor the transfer of LD proteins upon zygote formation. The results of this analysis indicate that ER fusion between mating partners is required for transfer of LD proteins and that this transfer is continuous, bidirectional and affects most LDs simultaneously. These observations suggest that LDs do not fuse upon mating of yeast cells, but that they form a network that is interconnected through the ER membrane. Consistent with this, ER-localized LD proteins rapidly move onto LDs of a mating partner and this protein transfer is affected by seipin, a protein important for proper LD biogenesis and the functional connection of LDs with the ER membrane.

Introduction

Lipid droplets (LDs) are intracellular compartments dedicated to the storage of neutral lipids, particularly triacylglycerol and steryl esters. They form globular structures composed of a hydrophobic core of neutral lipids that is shielded from the aqueous cytoplasm by a monolayer of phospholipids onto which a specific set of proteins associate. The structure of LDs is thus reminiscent of that of lipoproteins; however, unlike lipoproteins, LDs are not secreted. LD biogenesis is driven by the synthesis of neutral lipids by enzymes that are localized in the membrane of the endoplasmic reticulum (ER) (Olzmann and Carvalho, 2018, Thiam et al., 2013). LDs thus form from the ER membrane with which they remain closely associated throughout their life cycle, both in yeast and mammalian cells (Choudhary et al., 2015, Choudhary et al., 2020, Choudhary and Schneiter, 2021, Jacquier et al., 2011, Wilfling et al., 2013).

LD growth and expansion can occur by different pathways (Barneda and Christian, 2017). LDs expand through the localized synthesis of neutral lipids by enzymes such as Dga1/DGAT2 on the surface of or in the immediate vicinity to LDs (Jacquier et al., 2011, Kassan et al., 2013, Kuerschner et al., 2008, Wilfling et al., 2013, Xu et al., 2012). In addition, small LDs can fuse with each other to yield larger LDs (Bostrom et al., 2007, Gao et al., 2017a). Alternatively, LDs can grow through a ripening process, i.e., the incorporation of neutral lipids from either the ER or from adjacent LDs into pre-existing LDs (Jüngst et al., 2013, Salo et al., 2019, Thiam and Forêt, 2016).

Proteins localize to the surface of LDs through two distinct targeting determinants, amphipathic helices or hairpin-type of membrane domains (Dhiman et al., 2020, Kory et al., 2016). Hairpin-anchored proteins such as the diacylglycerol acyltransferase Dga1 in yeast, DGAT2 in mammalian cells, or the glycerol-3-phosphate acyltransferase 4 (GPAT4), are first targeted to the ER membrane from where they then localize to the surface of LDs (Jacquier et al., 2011, Olarte et al., 2020, Wilfling et al., 2013, Xu et al., 2012). Therefore, in the absence of LDs, these proteins are localized to the ER bilayer membrane but they prefer a triacylglycerol covering monolayer membrane over a pure phospholipid bilayer membrane *in vitro* (Caillon et al., 2020, Jacquier et al., 2011). The second class of LD-localized proteins, on the other hand, are more soluble and their amphipathic helices target the surface of LDs from the cytoplasm, possibly by recognizing lipid packing defects on the limiting

phospholipid monolayer of LDs. They include the abundant LD scaffolding perilipin family of proteins (PLIN) and their yeast orthologue Pet10, but also the Parkinson's disease associated protein alpha-synuclein (Bulankina et al., 2009, Chorlay and Thiam, 2020, Copic et al., 2018, Gao et al., 2017b, Jacquier et al., 2013, Prévost et al., 2018, Rowe et al., 2016, Sztalryd and Brasaemle, 2017).

Here we analyze the *in vivo* dynamics of proteins targeting to LDs using a yeast mating-based microscopic assay in which one of the mating partners expresses an mCitrine-tagged LD protein and the other cell expresses an mCherry-tagged LD protein together with a cytoplasmic cyan fluorescent protein (CFP). Three color time-lapse imaging allows us to analyze the redistribution of these marker proteins upon zygote formation. The results of these analyses indicate that LD proteins redistribute between LDs of mating cells in a continuous and bidirectional process which involves the majority of LDs in the mating pair. In cells where otherwise LD-localized proteins are mis-localized to the ER, we observe that these proteins reach the LDs of the mating partner through the interconnecting ER. LD-targeting of such proteins is delayed in mutants affecting ER fusion. Efficient ER to LD targeting requires seipin, an ER protein that is important for proper LD biogenesis and localizes to ER-LD contact sites. These results support a model in which LDs form a network of discrete compartments that are interconnected through the ER membrane through which they exchange their proteins with each other.

Results

Experimental design to monitor the transfer of proteins between LDs *in vivo*

To monitor the targeting of proteins to LDs, we adapted a yeast mating-based experimental setup (Anwar et al., 2012). Therefore, LD-marker proteins such as Erg6, an enzyme of the late part of the ergosterol biosynthetic pathway, or Dga1, a diacylglycerol acyltransferase which catalyzes the formation of TAG, were fused to fluorescent proteins and their expression was controlled by a galactose inducible promoter ($GAL1^{prom}$) (Gaber et al., 1989, Oelkers et al., 2002, Sorger and Daum, 2002). Plasmids encoding $GAL1^{prom}$*-ERG6-mCITRINE* or $GAL1^{prom}$*-DGA1-3mCHERRY* were then transformed into wild-type cells of different mating-type. *MAT*a cells expressing *DGA1-3mCHERRY* also co-expressed a soluble cytoplasmic

CFP, which served to monitor mixing of the cytoplasmic content between the two mating partners upon cell fusion, thereby defining the zero timepoint (t=0 min) of the mating reaction. Cells of both mating types were cultivated overnight in galactose containing media to induce expression of the fluorescently-tagged LD marker proteins. They were then resuspended in glucose-containing media to repress expression of the marker proteins, and mixed in a 1:1 ratio to initiate the mating reaction. After 2 h of co-cultivation, cells were mounted under an agarose patch on a glass coverslip and progression of mating reactions was monitored by time-lapse fluorescence microscopy (Fig. 1A). Before cell fusion occurred, Dga1-3mCherry was localized to punctuate LDs in cells expressing cytosolic CFP whereas Erg6-mCitrine marked punctuated LDs in cells that were negative for CFP fluorescence (Fig. 1A, t=-1 min). A line scan through a mating pair confirmed that Erg6-mCitrine fluorescence was confined to one half of the pre-zygote and Dga1-3mCherry and CFP fluorescence were both restricted to the other half. Upon cytoplasmic mixing, however, CFP fluorescence re-distributed throughout the zygote, while the two LD markers, Dga1-3mCherry and Erg6-mCitrine remained spatially separated (Fig. 1A, t=0 min). 40 min after cell fusion had occurred, the two LD markers colocalized on punctuate intracellular structures representing LDs as indicated by the overlap between red and green signals in the line scan and the appearance of a yellow signal in the merge (Fig. 1A, t=40 min). Thus, LD localized marker proteins started to colocalize on LDs of mating partners in a process that is much slower than cytoplasmic mixing.

To examine whether LD-localization of the fluorescent LD marker proteins was possibly due to their transfer through the aqueous space from a mating donor to an acceptor LD or due to their synthesis within the resulting zygote, we determined the half-life of these marker proteins upon glucose-dependent repression of the *GAL1*^{prom} and examined the solubility of these proteins by differential centrifugation. While both Dga1-3mCherry and Erg6-mCitrine were stably expressed in cells grown in the presence of galactose, glucose repression of their transcription resulted in a rapid decline of steady-state levels of Dga1-3mCherry, with a half-life of 31 min. Erg6-mCitrine was more stable even in glucose repressed cells, with half-life of 270 min (Fig. 1B). Both proteins cofractionated with Sec63, a component of the ER translocon, indicating that they are membrane-associated and thus are not likely to transfer through the shared cytoplasm of mating partners (Fig. 1C). Taken together these data indicate that pre-existing LD-localized proteins redistribute between donor

and acceptor LDs upon cell fusion, possibly through membrane-mediated protein transfer or through direct fusion of LDs between the mating partners.

Exchange of LD proteins between mating partners is continuous and reciprocal

Next, we analyzed the time-dependence of transfer of LD proteins between donor and acceptor. Therefore, time-lapse images of mating cells were recorded at 1 min intervals. The changes in fluorescence intensities of the fluorophores was measured in both mating partners and expressed as a percentage of whole cell intensity averaged over 5 time points prior to cytoplasmic mixing (t =-5 min to t=-1 min). This analysis revealed that the fluorescence of both Dga1-3mCherry and Erg6-mCitrine continuously increased over a period of approximately 20 min in the respective acceptor mating partner and then began to level off. This indicates that these LD-marker proteins redistributed between LDs of the two mating partners until they reached a new steady-state distribution in which all of the LDs in the resulting zygote were covered by both marker proteins (Fig. 2). Both marker proteins displayed similar behavior in this assay, suggesting that this transfer kinetics is not protein specific but possibly a more general property of membrane-associated LD proteins, yet the ratio between the ER- and LD-localization might vary between different proteins. Redistribution of these LD markers was reciprocal between the two mating partners as the increase in one of the marker proteins in the acceptor cell was paralleled by a concurrent decrease in fluorescence in the donor cell (Fig. 2C). At the qualitative level, this reciprocal exchange of LD proteins between LDs of the two mating partners was also observed in time-lapse images, which revealed that individual LDs acquired the respective LD marker from the mating partner with similar kinetics (Fig. 2B, time points 10 and 14 min, Movie S1). Analysis of the transfer of a genomically tagged version of Erg6 during mating revealed a dynamic similar to that of the galactose promoter controlled Erg6-mCitrine. In this case, however, a continuous increase of the fluorescence on the acceptor LDs was observed at later time points, because the synthesis of the protein was not repressed (Figure S1A, B). The continuous and reciprocal exchange of LD proteins between the two partners suggests that transfer occurs through membrane bridges connecting the LDs within the zygote rather than by LD-LD fusion. Fusion between LDs would likely result in a non-homogenous, mosaic-like, distribution of the marker proteins over

different LDs because not all the LDs would be expected to fuse simultaneously, resulting in LDs decorated with both fluorophores next to LDs that would show only red or only green fluorescence. This was not observed, supporting the notion that LDs did not fuse with each other upon mating of cells, but that they exchanged and re-equilibrate their protein content. Although the time resolution of imaging does not allow to unambiguously track the fate of a single LD, their dynamics and presence at the fusion neck suggest that LDs can also move from one half of the zygote to the other (Movie S1). To monitor this possible redistribution of LDs, rather than the transfer of LD markers, upon zygote formation, we labelled LDs with Pet10-mScarlet in one of the mating partners. When compared to the membrane anchored LD proteins Erg6 or Dga1, the soluble Pet10-mScarlet was less efficiently targeted to the LD surface of the mating partner. As consequence, two separate populations of LDs were discernible even 40 min after cytoplasmic mixing had occurred (Figure S1C, D). These observations indicate that at early time points of zygote formation, LDs appear to largely remain in the part of the zygote where they originate from.

Transfer of ER proteins precedes the exchange of LD proteins upon zygote formation, while the exchange of mitochondrial markers is comparatively slow

To examine whether the exchange of proteins between LDs of the newly formed zygote could be mediated by formation of a common ER membrane, we first analyzed the redistribution of an ER membrane protein, Sec63-mCherry, upon zygote formation. Sec63-mCherry fluorescence continuously increased in the acceptor cell and reached a plateau after approximately 20 min of cytoplasmic mixing (Fig. 3A-C, Movie S2). This time-dependence and the redistribution of Sec63-mCherry between donor and acceptor cells was slightly faster compared to the transfer of the LD marker Erg6-mCitrine. The soluble cytoplasmic marker CFP, on the other hand, very rapidly mixed with the cytoplasm of the mating partner to reach a new steady-state distribution in the zygote within approximately 1 min of cell fusion (Fig. 3C). Mitochondria, as monitored by a soluble MITO-3mCherry matrix protein, on the other hand, did not fuse to a significant degree with the organelle of the mating partner within this 20 min time-frame. However, at later time points, mitochondria started to appear in some of the acceptor cells, as indicated by a sudden increase of the standard deviation derived from monitoring 10 individual mating reactions (Fig.

3D-F, Movie S3) (Nunnari et al., 1997). Taken together, these observations suggest that LD proteins continuously and reciprocally exchange between the LDs of a newly formed zygote in a time-dependence that is more similar to the exchange of ER proteins than that of mitochondrial fusion and/or transfer.

The exchange of LD proteins between mating partners is strongly reduced in mutants that affect ER fusion

Next, we tested whether ER fusion between the mating partners is required for the exchange of LD proteins. Therefore, we analyzed the transfer of LD marker proteins in mutant cells known to exhibit a delay in homotypic ER fusion. These mutants bear defects in the yeast ortholog of atlastin, Sey1, a dynamin-like GTPase required for ER fusion, and in the Dsl1 tethering complex. These *sey1*Δ *dsl1*Δ*E* double mutants have previously been shown to reduce ER fusion in bi-parental matings, in which both mating partners are deficient for Sey1 and Dsl1 (Rogers et al., 2014). Mating of *sey1*Δ *dsl1*Δ*E* mutant cells expressing Dga1-3mCherry with *sey1*Δ *dsl1*Δ*E* mutant cells expressing Erg6-mCitrine resulted in a significantly slower initial rate of exchange of the two LD proteins between the mating partners. Moreover, time-lapse images indicate that the marker proteins did not significantly colocalize even after 20 min of cytoplasmic mixing (Fig. 4A, C, Movie S4). Colocalization of the two LD proteins was stalled at the mating neck, where ER membranes appeared to accumulate. This is likely due to the severe structural defects of the ER in *sey1*Δ *dsl1*Δ*E* mutant cells, which are known to accumulate ER at the bud neck (Fig. 4B) (Rogers et al., 2014). These results indicate that mutations that delay ER fusion also reduce the exchange of LD-localized proteins between mating partners, suggesting that ER fusion is required for efficient exchange of these LD proteins.

The delay in ER fusion in *sey1*Δ *dsl1*Δ*E* mutant cells was confirmed by analyzing the transfer of the ER luminal protein ss-mCherry-HDEL, a signal-sequence (ss) containing mCherry bearing a C-terminal ER retention signal (HDEL) (Fig. 4D) (Pelham et al., 1988). The averaged transfer curve of ss-mCherry-HDEL showed only a moderate delay in these mutant cells, probably due to the heterogeneity in the initiation of ER fusion during mating (Rogers et al., 2014). However, in recordings of single mating events the delay in transfer of the ER marker is more clearly visible, confirming the ER fusion phenotype (Fig. 4E). Taken together, these

results indicate that the efficient transfer of proteins between LDs of mating partners is delayed in mutants that affect ER fusion and thus likely depends of the formation of a common and continuous ER membrane between the mating partners upon zygote formation.

LD proteins are transferred from the ER membrane of one mating partner to LDs of a recipient

To examine whether the exchange of proteins between LDs of mating cells occurs via the ER membrane, we first tested whether LD proteins could relocalize from the ER membrane of a donor cell onto LDs of a mating partner. Cells lacking the four enzymes for neutral lipid biosynthesis, Are1 and Are2 for the synthesis of steryl esters, and Dga1 and Lro1 for the synthesis of TAG, have no detectable LDs (Sandager et al., 2002). In these quadruple mutant cells (*are1*Δ *are2*Δ *dga1*Δ *lro1*Δ) membrane associated proteins that are normally present on LDs are localized to the ER membrane (Jacquier et al., 2011). To test whether these ER-localized LD residents would relocalize from the ER of a donor onto LDs of a recipient, we analyzed mating between quadruple mutant cells expressing ER-localized Erg6-mCitrine and wild-type cells expressing Dga1-3mCherry. In the resulting zygotes, Erg6-mCitrine was transferred onto acceptor LDs in a very similar manner to what we previously observed for the exchange of LD proteins between wild-type cells (Fig. 5A, B, Movie S5). Concurrently, Dga1-3mCherry also redistributed from the donor cell into the ER of the recipient lacking LDs, suggesting that LD proteins continuously equilibrate between their LD- and ER-localization (Fig. 5, Movie S5). Under these conditions, transfer of ER-localized Erg6-mCitrine to the mating partner seemed to precede that of the LD-localized Dga1-3mCherry (Fig. 5C).

Following mating, Erg6-mCitrine labelled punctate structures quickly appeared in the ER of the recipient quadruple mutant. The rapid appearance of such newly formed LDs is likely due to the redistribution of neutral lipid biosynthetic enzymes from the ER of the wild-type partner into the ER of the quadruple mutant, as is indeed observed with mCherry labelled Dga1, a TAG biosynthetic enzyme (Fig. 5, Movie S5). In addition, neutral lipids contained within the ER membrane of the wild-type donor could diffuse into the quadruple mutant mating partner upon ER fusion, and thereby contribute to the emergence of LDs. Taken together, these results indicate that

LD proteins redistribute between their ER- and LD-localization upon fusion of the ER membranes of the mating partners.

LD proteins quickly move from the ER to LDs, but only slowly dissociate from LDs

To examine the exchange of LD-localized proteins between their ER localization and their LD association in more detail, we analyzed the exchange of Erg6-mCitrine and that of the ER luminal protein ss-mCherry-HDEL in different mating combinations between wild-type and *4*Δ (*are1*Δ *are2*Δ *dga1*Δ *lro1*Δ) cells (Fig. 6A-D). The resulting transfer curves for individual mating events were plotted and fitted to the Hill equation (Fig. 6E, F). From this mathematical modelling of single transfer curves, we could calculate the half-time of transfer of Erg6-mCitrine and ss-mCherry-HDEL (Fig. 6G). While the median half-times of transfer of ss-mCherry-HDEL are similar for all mating combinations, ranging from 1.5 to 2.4 min, the transfer rates of Erg6-mCitrine fell into two separate groups. The first group contained mating events in which Erg6-mCitrine was transferred from the ER to the ER (ER->ER, 5.2 min, i.e., mating between two *4*Δ mutant cells, *4*Δ x *4*Δ) or from the ER onto LDs (ER->LD, 6.4 min, i.e., mating between *4*Δ mutant cells and wild-type, *4*Δ x WT). The second group was composed of mating events in which Erg6-mCitrine had to dissociate from a donor LD to localize on an acceptor LD (LD->LD, 11.4 min, i.e., mating between two wild-type cells, WT x WT) or in which Erg6-mCitrine moved from LDs into the ER (LD->ER, 12.2 min, i.e., mating between wild-type and *4*Δ mutant, WT x *4*Δ). The differences in the median transfer rates between these two groups were statistically significant, indicating that the association of the protein from the ER onto LDs is about twice as fast as its dissociation from LDs into the ER. These data thus suggest that the relative affinity of Erg6 for LDs is higher than its affinity for the ER membrane.

Seipin affects the exchange of proteins between the ER and LDs

Seipin is an ER membrane protein required for proper formation of LDs. In the absence of seipin, cells either have many small clustered LDs, or they form large supersized LDs. Seipin forms disk-shaped oligomeric structures within the ER membrane at the base of LDs and thereby connects LDs to the ER membrane (Salo et

al., 2020). To examine whether seipin is also important for the exchange of proteins between the two compartments, we analyzed the exchange of Dga1-3mCherry and Erg6-mCitrine between LDs of mating partners lacking seipin. Both Dga1-3mCherry and Erg6-mCitrine relocated from one seipin mutant (*fld1*Δ) mating partner to the other (Fig 7A, B), yet they both appeared on LDs of the mating partner with some delay when compared to wild-type cells (Fig 7A, Movie S6). To quantify this delay, we analyzed the appearance of Dga1-3mCherry on Erg6-mCitrine containing acceptor LDs by calculating the ratio between Erg6-mCitrine and Dga1-3mCherry over time (Fig. 7C). Starting from 10 min of cytoplasmic mixing, this ratio was significantly elevated in wild-type compared to seipin mutant cells, indicating that seipin affects transfer of proteins between LDs of the two mating partners. Furthermore, heterogenous labelling of the LD population was observed in the seipin mutant, supporting the hypothesis that cargo delivery was impaired due to aberrant formation of ER-LD contact sites (Grippa et al., 2015, Salo et al., 2016). While exchange of both Dga1-3mCherry and Erg6-mCitrine is reduced in seipin mutant cells, the exchange of the ER marker ss-mCherry-HDEL was not affected during mating of seipin mutant cells (Fig. S2).

Seipin complexes are stable and do not mix upon zygote formation

To monitor the distribution of seipin upon zygote formation, we tagged seipin genomically with 2x mCherry (*FLD1-2mCHERRY*) and mated these cells with wild-type cells expressing Erg6-mCitrine. Before zygote formation, seipin was detectable as single puncta. Upon zygote formation, these seipin puncta started to become decorated with Erg6-mCitrine, indicating that Erg6-mCitrine re-equilibrated its distribution to localize to pre-existing LDs from the mating partner (Fig. 8A, B, Movie S7).

To address whether seipin itself would mix and colocalize with the seipin complex of the mating partner, we tagged seipin genomically with a 7x concatenated split variant of GFP ($GFP11_{x7}$) and expressed the remaining part of GFP (GFP1-10) from a plasmid (Kamiyama et al., 2016). Both color variants of seipin localized to the base of Bodipy-stained LDs and the mCherry-tagged seipin defined the site of LD formation when quadruple mutant cells lacking LDs (4Δ, *are1*Δ *are2*Δ *dga1*Δ *lro1*Δ) were mated with wild-type cells expressing Erg6-mCitrine (Fig. S3). When cells

expressing the red-fluorescently tagged seipin (Fld1-2mCherry) were mated with cells expressing the split-GFP variant of seipin, the red and green fluorescent puncta appeared to remain stable with hardly any colocalization within a 40 min time-frame after cytoplasmic mixing (Fig. 8C, Movie S8). This degree of non-colocalization in the zygote was similar to that observed when haploid cells of the same mating type, expressing these two color-variants of seipin were mixed (Fig. 8C, D, no mating). On the other hand, when the two color-variants of seipin were simultaneously expressed in a diploid cell, clear colocalization was observed (Fig. 8C, D, diploid). Similarly, zygote formation between cells expressing Dga1-3mCherry and Erg6-mCitrine resulted in rapid colocalization of these two LD-markers, but they remained separated when haploid cells of the same mating type were mixed, but colocalized when simultaneously expressed in a diploid (Fig. 8C). Quantification of the colocalization of the two color-variants of seipin in comparison to the two LD markers indicates that seipin spots do not mix between mating partners upon zygote formation (Fig. 8D). Thus, taken together, unlike the membrane anchored LD marker proteins, Dga1 and Erg6, which rapidly re-equilibrate their LD localization upon zygote formation, seipin puncta remained stable and did not exchange monomers upon merging of the ER membrane between the two mating partners.

Discussion

In this study, we analyzed the transfer of LD proteins between mating pairs *in vivo*. This transfer is continuous, and reciprocal and appears to simultaneously occur on the majority of LDs of the newly formed zygote. This indicates that these proteins rapidly re-equilibrate their localization to reach a new steady-state distribution within approximately 20 min of cytoplasmic mixing (Fig. 1, 2). The two membrane-anchored LD proteins Dga1 and Erg6 tested here displayed similar transfer rates, suggesting that the observations made are likely valid for a wider range of proteins containing a hydrophobic hairpin type of LD-targeting determinant (Fig. 2). These LD proteins thus re-equilibrate their distribution at a rate that is slower than the re-equilibration of an ER residential protein, such as Sec63 (Fig. 3). However, re-equilibration is strongly delayed in mutants with defects in homotypic ER fusion, i.e., *sey1*Δ *dsl1*Δ*E*, suggesting that transfer of the LD proteins occurred through an interconnecting ER

membrane (Fig. 4). Consistent with this proposition, transfer of ER-localized LD proteins from cells that have no LDs, i.e., *4*Δ mutant cells lacking all four enzymes required for neutral lipid synthesis (*are1*Δ *are2*Δ *dga1*Δ *lro1*Δ), to the LDs of a mating partner occurs at a rate that is almost twice as fast as the transfer between LDs (Fig. 5, 6). These data indicate that LD proteins are in a constant equilibrium between their ER and LD localization and that they associate more readily from the ER membrane with the LD surface than they dissociate back from the LD surface into the ER membrane. Taken together, these observations suggest that LDs form a network of compartments that are interconnected through the ER membrane. The data, on the other hand, do not support a model where LDs stay disconnected from the ER membrane for an extended period of time and in which the transfer of LD proteins would require homotypic LD-LD fusion. The network model is also supported by the observation that seipin is required for efficient transfer of LD proteins, because seipin localizes to and likely even forms the connection between the ER membrane and LDs (Choudhary and Schneiter, 2021, Salo et al., 2020).

A model of LDs forming a network of compartments interconnected by the ER membrane is consistent with previous observations showing uniform incorporation of TAG into existing LDs by quantitative electron microscopy (EM) and fluorescent microscopy using fluorescent polyene lipids in living cells (Cheng et al., 2009, Kuerschner et al., 2008). Similarly, polarized flow cytometry indicates that newly synthesized steryl esters are incorporated from the ER into pre-existing LDs rather than forming new droplets (Kellner-Weibel et al., 2001). In addition, label free holo-tomographic microscopy indicates that newly formed LDs are created at the expense of older LDs, indicating that LDs exchange material over relatively short timescales, possibly through an interconnecting ER membrane (Sandoz et al., 2019).

Our data indicate that seipin is required for efficient exchange of LD proteins upon zygote formation (Fig. 7). Seipin has previously been shown to be important to control lipid exchange through a process termed ripening, i.e., the transfer of lipids between adjacent LDs through the interconnecting ER membrane. Thereby seipin ensures uniform LD growth and controls the size distribution of the LD population (Salo et al., 2019). In addition, seipin mutant cells, have an altered composition of the LD membrane and the LD proteome and thus fail to properly establish LD identity (Grippa et al., 2015, Salo et al., 2016). Seipin is thus important to control the exchange of both lipids and proteins between the ER membrane and LDs (Salo et al.,

2020). In the absence of seipin, LDs are formed at ectopic sites through the ER membrane, indicating that seipin controls both initiation of LD formation as well as their subsequent growth (Choudhary et al., 2020). The observation that seipin complexes do not mix upon ER fusion and zygote formation indicates that the seipin ring complex is stable and that there is no or little exchange of monomers between the oligomeric ring-complexes (Fig. 8). Hairpin-anchored LD proteins, however, do exchange between LDs suggesting that they can traverse through the stable seipin-mediated connection between the ER membrane and the LD surface. LD-targeted proteins that are anchored to the ER membrane through one or multiple transmembrane domains, however, cannot diffuse onto the LD surface, indicating that the ER-LD interface is transparent for hairpin-anchored proteins only (Khaddaj et al., 2022).

Targeting of protein to the LD surface has been proposed to be limited by protein crowding, i.e., the saturation of all available LD surface cues through binding to proteins. Under such crowding conditions, newly made LD proteins could no longer localize to the LD surface and hence would possibly either be degraded or stay in the ER membrane (Ruggiano et al., 2016). We observe a flattening of the transfer curve after approximately 20 min of zygote formation and believe that this reflects a newly reached steady-state distribution of the LD proteins rather than a saturation of the capacity of the LD surface to acquire more protein. This interpretation is supported by the observation that the acceptor cell continues to acquire more of the LD marker under conditions of continued protein synthesis, i.e., when Erg6-mCitrine is controlled by its native promoter (Fig S1A, B). Both LD marker proteins used in this study are overexpressed from a strong galactose regulated promoter and the promoter is turned off 2 h before cells are mated, both markers are being targeted apparently quantitatively to the LD of the recipient cell with only a small fraction remaining visible in the ER membrane. This suggests that the capacity of the LD surface to host these markers is not limiting. Similarly, in mating with *4*Δ mutant cells, the LD marker that resides in the ER of the quadruple mutant is targeted seemingly quantitatively to the LD surface of the recipient mating partner. Thus, under these dynamic *in vivo* conditions, molecular crowding on the LD surface does not appear to limit the capacity of the LD to adapt its surface proteome. This situation, however, may change upon induction of lipolysis and shrinkage of the LD surface, resulting in displacement of surface proteins (Kory et al., 2015).

Why and how exactly do these membrane anchored proteins equilibrate their LD localization upon mating and fusion of the ER membranes ? While under non-mating conditions, it is likely that the shrinkage of LDs due to lipolysis induces a relocalization of the LD markers back into the ER membrane, the situation under the mating conditions analyzed here, are likely different. The mating reactions is accompanied by homotypic fusion of the ER membranes between the two mating partners. This ER fusion is required for efficient re-equilibration of the LD markers. Could this ER fusion induce conditions that are comparable to those observed under lipolysis? Karyogamy is typically followed by a rapid cell division requiring membrane proliferation. However, even if zygote formation would induce lipolytic conditions, this could only account for the relocalization of the LD marker protein from its LD localization back to an ER localization, but not for the apparent uniform and bidirectional transfer between the LDs of the two mating gametes. It seems possible that not only the membrane anchored LD-localized proteins re-equilibrate upon ER fusion but that this protein exchange is actually accompanied by a similar re-equilibration of the neutral lipid content of these LDs. In that case, both membrane anchored proteins and neutral lipids could diffuse through the newly formed common ER membrane, acting as a solvent, to catalyze a new steady-state distribution of the LD content. How this re-equilibration is driven is unclear, but it seems possible that membrane tension and Ostwald ripening could promote such a process (Salo et al., 2019, Thiam and Forêt, 2016).

The mating-based readout established here, will likely be helpful to monitor the time dependent transfer of lipids and proteins to the ER-LD interface and the LD surface in living cells. Thereby, this *in vivo* assay might help to unravel processes that govern the initiation of LD formation, maintenance of LDs and their turnover, and also the mechanisms that coordinate the expansion and growth of this interconnected network of lipid stores.

Acknowledgements

We thank all members of the lab for support, advice and helpful discussions and Aslihan Ekim Kocabey for comments on the manuscript, Shirish Mishra for initial help setting up the microscopic readout, Rudolf Rohr for advice on statistical

analysis and the Hill equation, and the Light Microscopy and Bioimage Informatics Facility of the University of Fribourg for support and assistance in this work. We also thank Jodi Nunnari, Mark Rose, and Andreas Conzelmann for antibodies, plasmids and strains. This work is supported by the Swiss National Science Foundation (31003A_173003).

Conflicts of Interests

The authors declare to have no conflicts of interests.

Material and methods

Yeast strains, growth media, and plasmid preparation

Yeast strains were cultivated in minimal defined media containing 0.67% yeast nitrogen base without amino acids (US Biological), 0.73 g/l amino acids, and 2% carbon source i. e. glucose, raffinose or galactose, depending on the need (US Biological).

Strains used in this study are listed in Table S1. Starting from the Euroscarf single mutants of the 4 genes involved in the final step of neutral lipid biosynthesis: *ARE1, ARE2, DGA1, LRO1,* the *MAT*α *are1*Δ *are2*Δ *dga1*Δ *lro1*Δ quadruple mutant strain was obtained after a series of mating, sporulation and assessment of genotypes by PCRs. Mating type was determined by crossing the candidate strains with tester strains *MAT*α *thr* and *MAT*a *thr* and analyzing the auxotrophy of the diploid. *MAT*α cells were then transformed with plasmid pGAL-HO for mating type switching (Herskowitz and Jensen, 1991). Diploid cells were obtained by crossing haploid cells and selected in the appropriate minimal media. *MAT*a and *MAT*α *sey1*Δ *dsl1*Δ*E* were obtained by sporulation of the strain MY14769 (a kind gift from Mark Rose) and the genotype of spores was determined by growing cells on selective media.

ERG6-mCITRINE^{A206K} was obtained by PCR ligation to fuse *ERG6* and *mCITRINE* and introduce the mutation A206K to favor monomeric Citrine (Shaner et al., 2005). The PCR product was recombined into the SalI site of plasmid pGREG506. Then the whole expression cassette *GAL1*^{prom}*-ERG6-mCITRINE*^{A206K} was amplified by PCR and recombined into plasmid pRS415 to switch the selectable marker from

URA3 to *LEU2*. The endogenously tagged version of *ERG6*-m*CITRINE*^{A206K} was obtained by genomic integration of the *mCITRINE*^{A206K}*-CaURA3* cassette. The *3mCHERRY* cassette was amplified from plasmid p30648 (Dultz and Ellenberg, 2010), and recombined into the XhoI site of pGREG600 to replace GFP and yield *GAL1*^{prom}*-RecombinationSite-3mCHERRY* (p1079). This plasmid was then used to obtain 3mCherry fusion proteins under the control of *GAL1* promoter for tagging *DGA1* and *SEC63*, yet due to recombination, *SEC63* was only tagged with mCherry. Coding sequences of interest were amplified from yeast DNA. The *Neurospora crassa ATP9* mitochondrial targeting sequence (Westermann and Neupert, 2000) was amplified from the plasmid MITO-RFP, and also recombined into p1079 to label mitochondria. To target mCherry to the ER lumen under the control of a galactose-inducible promoter, *PRC1*^{ss}*-mCHERRY-HDEL* was PCR-amplified from plasmid MR6474 (Rogers et al., 2014) and recombined into pGREG503 digested with SalI restriction enzymes. Amplification of *sfGFP1-10* from plasmid #129416 (Addgene; (Salo et al., 2019)) and recombination into the XmaI site of plasmid pRS416-ADH1 yielded a plasmid for expression of sfGFP1-10 from the *ADH1* promoter. A similar strategy was used for the expression BFP whose coding sequence was recombined into pRS415-ADH1.

To genomically tag Fld1 with multiple mCherry, a tagging cassette obtained by PCR was recombined into the *FLD1* locus. PCR was used to add recombination arms for insertion into the genome and to PCR-ligate *mCHERRYs* amplified from plasmid p1079 with *SpHIS5* selection marker amplified from the pKT vectors (Jansen et al., 2005). With this strategy we obtained strains *MAT*α *FLD1-2mCHERRY*, and *MAT*α *are1*Δ *are2*Δ *dga1*Δ *lro1*Δ *FLD1-3mCHERRY*. A similar approach was employed to fuse *FLD1* to *sfGFP11*$_{x7}$ amplified from plasmid #70224 (Addgene; (Kamiyama et al., 2016)). To visualize Fld1, the *FLD1-sfGFP11*$_{x7}$ strain should also expressed sfGFP1-10 (plasmid #p2212) to allow complementation of the two halves of the sfGFP. Plasmids used in this study are listed in Table S2.

Fluorescence microscopy

For microscopic analysis of yeast mating events, cells were first grown in raffinose supplemented selective media, and then shifted to galactose media for overnight cultivation. The next morning, the density of the cells was adjusted to OD_{600} = 0.7, and cells were further grown in galactose media (2 h). 1 ml of *MAT*a

cells and 1 ml of *MAT*α cells were collected together, and washed once with non-selective glucose medium. Cells were then resuspended in 1 ml of the same medium and incubated for 2 h at 30°C without shaking. Finally, cells were collected by centrifugation, resuspended in 50 μl medium, and 2 μl of the cell suspension was placed on a cover slip and overlaid with a SC-glucose-agarose patch to allow live cell imaging for up to 100 min at 25°C. The same procedure was used for monitoring strains expressing fluorescently tagged Fld1, except that cells were cultured in glucose media only.

For Bodipy staining, cells were collected at around OD 2, washed with PBS, and incubated at room temperature, in the dark for 30 min with Bodipy (2 µg/ml). The cells were then washed 2x with PBS, and directly imaged when treated with Bodipy 493/503 (Invitrogen), or cultivated for 2 h before imaging for Bodipy-C12 558/568 (Invitrogen).

To image mating events, a Visitron spinning disk CSU-W1 (Visitron Systems, Puchheim, Germany) was employed. It consists of a Nikon Ti-E inverted microscope, supplied with a CSU-W1 spinning disk head with a 50 μm pinhole disk (Yokogawa, Tokyo, Japan), a PLAN APO 10x NA 1.3 oil immersion objective (Nikon), and an Evolve 512 (Photometrics) EM-CCD camera. Single optical sections were acquired every minute, during 101 minutes, in mCherry, YFP and CFP channels with filter sets for YFP/CFP and mCherry recordings. We account the vibrations induced by the motorized change of filter sets for a slight displacement between color channels that are visible in some highly magnified recordings of live cells labelled with YFP/CFP and mCherry. For imaging strains with fluorescently tagged Fld1, the interval between acquisitions was set to 2 min, and when the 7x split sfGFP was analyzed, the CFP cytosolic marker was replaced by BFP and the mCherry, GFP and DAPI channels were used for image acquisition. The images were processed and analyzed using FIJI software (Schindelin et al., 2012), and resized in Adobe Photoshop. In line scan analysis, the intensity distribution of each fluorophore along a defined line was quantified, and total intensity was normalized to 1.

To follow the transfer of the different fluorescently tagged proteins, the increase in fluorescent signal in recipient cells was expressed as percentage of total fluorescence in the donor cell before cytoplasmic mixing had occurred. Cytoplasmic mixing was assessed by monitoring the presence of CFP in both mating partners.

To parameterize the transfer rate of Erg6-mCitrin, and ss-mCherry-HDEL during mating, the transfer curve (average Fig. 4E, or every mating events Fig. 4F) was fitted to the Hill equation: $y= T^{\delta} M/(h+T^{\delta})$, with the help of the Solver add-in in Excel. Half-life of transfer was calculated with the equation: $T½ = h^{(1/\delta)}$, as an estimate for the transfer rate of the fluorescent protein. Box plot and statistical analysis were performed with R (R Development Core Team, 2008), and the ggplot2 package (Wickham, 2016). Wilcoxon rank-sum test was used with Benjamini-Hochberg correction to assess the significance of data.

To estimate the transfer of Erg6-mCitrine to LDs in WT x WT or *fld1*Δ x *fld1*Δ mating, we plotted the ratio of relative intensity of Dga1-3mCherry on LDs to that of Erg6-mCitrine. The increase in ratio is both due to LDs gaining Dga1-3mCherry and losing Erg6-mCitrine over time.

The Pearson correlation factors were determined with the help of the Coloc2 Fiji plugin (Schindelin et al., 2012). Background was subtracted for each channel, and colocalization was analyzed in a region of interest consisting of a zygote or two adjacent cells. Due to weak signals, we plotted Pearson's R value with no threshold, and included positive and negative controls to evaluate the level of colocalization that is detectable in diploid cells expressing both fluorescent proteins (positive control) and in adjacent cells that were not undergoing mating (negative control).

Protein analysis

To analyze protein turnover following promoter shut off, yeast cells were grown essentially as described for microscopic imaging: preculture in raffinose selective medium, protein induction in galactose selective medium overnight, dilution to OD = 0.5 in galactose medium, growth for 2 h before separating the culture into two parts, one held in galactose medium, the other half supplied with glucose to turn expression of *GAL1* promoter driven marker proteins off. Cells were collected every hour, starting 1 h after dilution to OD = 0.5 (t=-1). At each time point, 3 OD_{600} units of yeast cells were collected, proteins were extracted, and precipitated with 10% TCA. For Western analysis, 0.5 OD_{600} units of cells were loaded, as described before (Choudhary and Schneiter, 2012). Protein levels were quantified, corrected with respect to the loading control, 3-phosphoglycerate kinase Pgk1, and expressed as percentage relative to t=0. Protein half-life was calculated by fitting the function

$N=N_0*e^{-kt}$ to the experimental data with the Solver add-in of Excel (Microsoft Corporation) and then using the equation: $T_{1/2}=\ln(2)/k$ (Belle et al., 2006).

Protein association with membrane was analyzed by differential centrifugation. 100 OD_{600} units of cells were collected after growth in galactose selective medium followed by 2 h in glucose supplemented medium. Cells were lysed in a buffer containing 0.2 M sorbitol, 50 mM potassium acetate, 20 mM HEPES (pH 6.8), 2 mM EDTA (pH 8.0), supplemented with protease inhibitor cocktail (Roche Diagnostics, Mannheim, Germany) and 0.2 mM phenylmethylsulfonyl fluoride (PMSF). Fractionation was performed as described before, except that the homogenate was only separated into a 30'000 g pellet (P) and soluble proteins (S) by centrifugation at 30'000 g for 30 min at 4°C (Köffel et al., 2005). Protein concentration in each fraction was determined by a Bradford assay, and 100 μg of proteins were precipitated with TCA and resuspended in loading dye. Subsequently, 10 μg of protein were loaded on SDS-PAGE and analyzed by Western blotting.

SDS-PAGE and Western blotting were performed according to standard protocols. The primary antibodies employed were: Purified anti-mCherry antibody (mouse, 1:1000, BioLegend # 677702), monoclonal anti-GFP (mouse, 1:2000, Roche # 11814460001), which also detected mCitrine-tagged proteins, anti-Pgk1 monoclonal antibody 22C5D8 (mouse, 1:5000, Invitrogen # 459250), anti-Ayr1 (rabbit, 1:5000, G. Daum, TU-Graz, Austria), anti-GAPDH (rabbit, 1:4000, G. Daum, TU-Graz, Austria), and anti-Sec63 (sheep, 1:10000, A. Conzelmann, University of Fribourg, and G. Forte, University of Manchester). As secondary antibodies goat anti-mouse IgG (H+L)-HRP conjugate (1:10000, Bio-Rad # 1706516), goat anti-rabbit IgG (H+L)-HPR conjugate (1:10000, Bio-Rad # 1706515), and anti-sheep IgG-HRP conjugate (1:10000, Sigma Aldrich # A3415) were employed.

References

Anwar, K., Klemm, R. W., Condon, A., Severin, K. N., Zhang, M., Ghirlando, R., Hu, J., Rapoport, T. A. and Prinz, W. A. (2012). The dynamin-like GTPase Sey1p mediates homotypic ER fusion in S. cerevisiae. *J Cell Biol.* **197,** 209-217.

Barneda, D. and Christian, M. (2017). Lipid droplet growth: regulation of a dynamic organelle. *Curr Opin Cell Biol.* **47,** 9-15.

Belle, A., Tanay, A., Bitincka, L., Shamir, R. and O'Shea, E. K. (2006). Quantification of protein half-lives in the budding yeast proteome. *Proc Natl Acad Sci U S A.* **103,** 13004-13009.

Bostrom, P. et al. (2007). SNARE proteins mediate fusion between cytosolic lipid droplets and are implicated in insulin sensitivity. *Nat Cell Biol.* **9,** 1286-1293.

Bulankina, A. V., Deggerich, A., Wenzel, D., Mutenda, K., Wittmann, J. G., Rudolph, M. G., Burger, K. N. and Honing, S. (2009). TIP47 functions in the biogenesis of lipid droplets. *J Cell Biol.* **185,** 641-655.

Caillon, L., Nieto, V., Gehan, P., Omrane, M., Rodriguez, N., Monticelli, L. and Thiam, A. R. (2020). Triacylglycerols sequester monotopic membrane proteins to lipid droplets. *Nat Commun.* **11,** 3944.

Cheng, J., Fujita, A., Ohsaki, Y., Suzuki, M., Shinohara, Y. and Fujimoto, T. (2009). Quantitative electron microscopy shows uniform incorporation of triglycerides into existing lipid droplets. *Histochem Cell Biol.* **132,** 281-291.

Chorlay, A. and Thiam, A. R. (2020). Neutral lipids regulate amphipathic helix affinity for model lipid droplets. *J Cell Biol.* **219,**

Choudhary, V., El Atab, O., Mizzon, G., Prinz, W. A. and Schneiter, R. (2020). Seipin and Nem1 establish discrete ER subdomains to initiate yeast lipid droplet biogenesis. *J Cell Biol.* **219,**

Choudhary, V., Ojha, N., Golden, A. and Prinz, W. A. (2015). A conserved family of proteins facilitates nascent lipid droplet budding from the ER. *J Cell Biol.* **211,** 261-271.

Choudhary, V. and Schneiter, R. (2012). Pathogen-Related Yeast (PRY) proteins and members of the CAP superfamily are secreted sterol-binding proteins. *Proc Natl Acad Sci U S A.* **109,** 16882-16887.

Choudhary, V. and Schneiter, R. (2021). A Unique Junctional Interface at Contact Sites Between the Endoplasmic Reticulum and Lipid Droplets. *Front Cell Dev Biol.* **9,** 650186.

Copic, A., Antoine-Bally, S., Giménez-Andrés, M., La Torre Garay, C., Antonny, B., Manni, M. M., Pagnotta, S., Guihot, J. and Jackson, C. L. (2018). A giant amphipathic helix from a perilipin that is adapted for coating lipid droplets. *Nat Commun.* **9,** 1332.

Dhiman, R., Caesar, S., Thiam, A. R. and Schrul, B. (2020). Mechanisms of protein targeting to lipid droplets: A unified cell biological and biophysical perspective. *Semin Cell Dev Biol.*

Dultz, E. and Ellenberg, J. (2010). Live imaging of single nuclear pores reveals unique assembly kinetics and mechanism in interphase. *J Cell Biol.* **191,** 15-22.

Gaber, R. F., Copple, D. M., Kennedy, B. K., Vidal, M. and Bard, M. (1989). The yeast gene ERG6 is required for normal membrane function but is not essential for biosynthesis of the cell-cycle-sparking sterol. *Mol Cell Biol.* **9,** 3447-3456.

Gao, G., Chen, F.-J., Zhou, L., Su, L., Xu, D., Xu, L. and Li, P. (2017a). Control of lipid droplet fusion and growth by CIDE family proteins. *Biochimica et Biophysica Acta (BBA)-Molecular and Cell Biology of Lipids.* **1862,** 1197-1204.

Gao, Q., Binns, D. D., Kinch, L. N., Grishin, N. V., Ortiz, N., Chen, X. and Goodman, J. M. (2017b). Pet10p is a yeast perilipin that stabilizes lipid droplets and promotes their assembly. *J Cell Biol.* **216,** 3199-3217.

Grippa, A., Buxó, L., Mora, G., Funaya, C., Idrissi, F. Z., Mancuso, F., Gomez, R., Muntanyà, J., Sabidó, E. and Carvalho, P. (2015). The seipin complex Fld1/Ldb16 stabilizes ER-lipid droplet contact sites. *J Cell Biol.* **211,** 829-844.

Herskowitz, I. and Jensen, R. E. (1991). Putting the HO gene to work: practical uses for mating-type switching. *Methods Enzymol.* **194,** 132-146.

Jacquier, N., Choudhary, V., Mari, M., Toulmay, A., Reggiori, F. and Schneiter, R. (2011). Lipid droplets are functionally connected to the endoplasmic reticulum in Saccharomyces cerevisiae. *J Cell Sci.* **124,** 2424-2437.

Jacquier, N., Mishra, S., Choudhary, V. and Schneiter, R. (2013). Expression of oleosin and perilipins in yeast promotes formation of lipid droplets from the endoplasmic reticulum. *J Cell Sci.* **126,** 5198-5209.

Jansen, G., Wu, C., Schade, B., Thomas, D. Y. and Whiteway, M. (2005). Drag&Drop cloning in yeast. *Gene.* **344,** 43-51.

Jüngst, C., Klein, M. and Zumbusch, A. (2013). Long-term live cell microscopy studies of lipid droplet fusion dynamics in adipocytes. *Journal of lipid research.* **54,** 3419-3429.

Kamiyama, D. et al. (2016). Versatile protein tagging in cells with split fluorescent protein. *Nat Commun.* **7,** 11046.

Kassan, A. et al. (2013). Acyl-CoA synthetase 3 promotes lipid droplet biogenesis in ER microdomains. *J Cell Biol.* **203,** 985-1001.

Kellner-Weibel, G., McHendry-Rinde, B., Haynes, M. P. and Adelman, S. (2001). Evidence that newly synthesized esterified cholesterol is deposited in existing cytoplasmic lipid inclusions. *J Lipid Res.* **42,** 768-777.

Khaddaj, R., Mari, M., Cottier, S., Reggiori, F. and Schneiter, R. (2022). The surface of lipid droplets constitutes a barrier for endoplasmic reticulum-resident integral membrane proteins. *J Cell Sci.* **135,** jcs256206.

Köffel, R., Tiwari, R., Falquet, L. and Schneiter, R. (2005). The Saccharomyces cerevisiae YLL012/YEH1, YLR020/YEH2, and TGL1 genes encode a novel family of membrane-anchored lipases that are required for steryl ester hydrolysis. *Mol Cell Biol.* **25,** 1655-1668.

Kory, N., Farese, R. V. and Walther, T. C. (2016). Targeting Fat: Mechanisms of Protein Localization to Lipid Droplets. *Trends Cell Biol.* **26,** 535-546.

Kory, N., Thiam, A. R., Farese, R. V. and Walther, T. C. (2015). Protein Crowding Is a Determinant of Lipid Droplet Protein Composition. *Dev Cell.* **34,** 351-363.

Kuerschner, L., Moessinger, C. and Thiele, C. (2008). Imaging of lipid biosynthesis: how a neutral lipid enters lipid droplets. *Traffic.* **9,** 338-352.

Nunnari, J., Marshall, W. F., Straight, A., Murray, A., Sedat, J. W. and Walter, P. (1997). Mitochondrial transmission during mating in Saccharomyces cerevisiae is determined by mitochondrial fusion and fission and the intramitochondrial segregation of mitochondrial DNA. *Mol Biol Cell.* **8,** 1233-1242.

Oelkers, P., Cromley, D., Padamsee, M., Billheimer, J. T. and Sturley, S. L. (2002). The DGA1 gene determines a second triglyceride synthetic pathway in yeast. *J Biol Chem.* **277,** 8877-8881.

Olarte, M. J., Kim, S., Sharp, M. E., Swanson, J. M. J., Farese, R. V. and Walther, T. C. (2020). Determinants of Endoplasmic Reticulum-to-Lipid Droplet Protein Targeting. *Dev Cell.* **54,** 471-487.e7.

Olzmann, J. A. and Carvalho, P. (2018). Dynamics and functions of lipid droplets. *Nat Rev Mol Cell Biol.* **20,** 137-155.

Pelham, H. R., Hardwick, K. G. and Lewis, M. J. (1988). Sorting of soluble ER proteins in yeast. *EMBO J.* **7,** 1757-1762.

Prévost, C., Sharp, M. E., Kory, N., Lin, Q., Voth, G. A., Farese, R. V. and Walther, T. C. (2018). Mechanism and Determinants of Amphipathic Helix-Containing Protein Targeting to Lipid Droplets. *Dev Cell.* **44,** 73-86.e4.

Rogers, J. V., McMahon, C., Baryshnikova, A., Hughson, F. M. and Rose, M. D. (2014). ER-associated retrograde SNAREs and the Dsl1 complex mediate an alternative, Sey1p-independent homotypic ER fusion pathway. *Mol Biol Cell.* **25,** 3401-3412.

Rowe, E. R. et al. (2016). Conserved Amphipathic Helices Mediate Lipid Droplet Targeting of Perilipins 1-3. *J Biol Chem.* **291,** 6664-6678.

Ruggiano, A., Mora, G., Buxó, L. and Carvalho, P. (2016). Spatial control of lipid droplet proteins by the ERAD ubiquitin ligase Doa10. *EMBO J.*

Salo, V. T., Hölttä-Vuori, M. and Ikonen, E. (2020). Seipin-Mediated Contacts as Gatekeepers of Lipid Flux at the Endoplasmic Reticulum–Lipid Droplet Nexus. *Contact.* **3,** 2515256420945820.

Salo, V. T. et al. (2016). Seipin regulates ER-lipid droplet contacts and cargo delivery. *EMBO J.* **35,** 2699-2716.

Salo, V. T. et al. (2019). Seipin Facilitates Triglyceride Flow to Lipid Droplet and Counteracts Droplet Ripening via Endoplasmic Reticulum Contact. *Dev Cell.*

Sandager, L., Gustavsson, M. H., Stahl, U., Dahlqvist, A., Wiberg, E., Banas, A., Lenman, M., Ronne, H. and Stymne, S. (2002). Storage lipid synthesis is non-essential in yeast. *J Biol Chem.* **277,** 6478-6482.

Sandoz, P. A., Tremblay, C., van der Goot, F. G. and Frechin, M. (2019). Image-based analysis of living mammalian cells using label-free 3D refractive index maps reveals new organelle dynamics and dry mass flux. *PLoS Biol.* **17,** e3000553.

Schindelin, J. et al. (2012). Fiji: an open-source platform for biological-image analysis. *Nat Methods.* **9,** 676-682.

Shaner, N. C., Steinbach, P. A. and Tsien, R. Y. (2005). A guide to choosing fluorescent proteins. *Nat Methods.* **2,** 905-909.

Sorger, D. and Daum, G. (2002). Synthesis of triacylglycerols by the acyl-coenzyme A:diacyl-glycerol acyltransferase Dga1p in lipid particles of the yeast Saccharomyces cerevisiae. *J Bacteriol.* **184,** 519-524.

Sztalryd, C. and Brasaemle, D. L. (2017). The perilipin family of lipid droplet proteins: Gatekeepers of intracellular lipolysis. *Biochim Biophys Acta Mol Cell Biol Lipids.* **1862,** 1221-1232.

Thiam, A. R., Farese, R. V. J. and Walther, T. C. (2013). The biophysics and cell biology of lipid droplets. *Nat Rev Mol Cell Biol.* **14,** 775-786.

Thiam, A. R. and Forêt, L. (2016). The physics of lipid droplet nucleation, growth and budding. *Biochim Biophys Acta.* **1861,** 715-722.

Westermann, B. and Neupert, W. (2000). Mitochondria-targeted green fluorescent proteins: convenient tools for the study of organelle biogenesis in Saccharomyces cerevisiae. *Yeast.* **16,** 1421-1427.

Wickham, H. 2016. *ggplot2: Elegant Graphics for Data Analysis*. Springer-Verlag New York. ISBN 978-3-319-24277-4,

Wilfling, F. et al. (2013). Triacylglycerol synthesis enzymes mediate lipid droplet growth by relocalizing from the ER to lipid droplets. *Dev Cell.* **24,** 384-399.

Xu, N., Zhang, S. O., Cole, R. A., McKinney, S. A., Guo, F., Haas, J. T., Bobba, S., Farese, R. V. J. and Mak, H. Y. (2012). The FATP1-DGAT2 complex facilitates lipid droplet expansion at the ER-lipid droplet interface. *J Cell Biol.* **198,** 895-911.

Figures

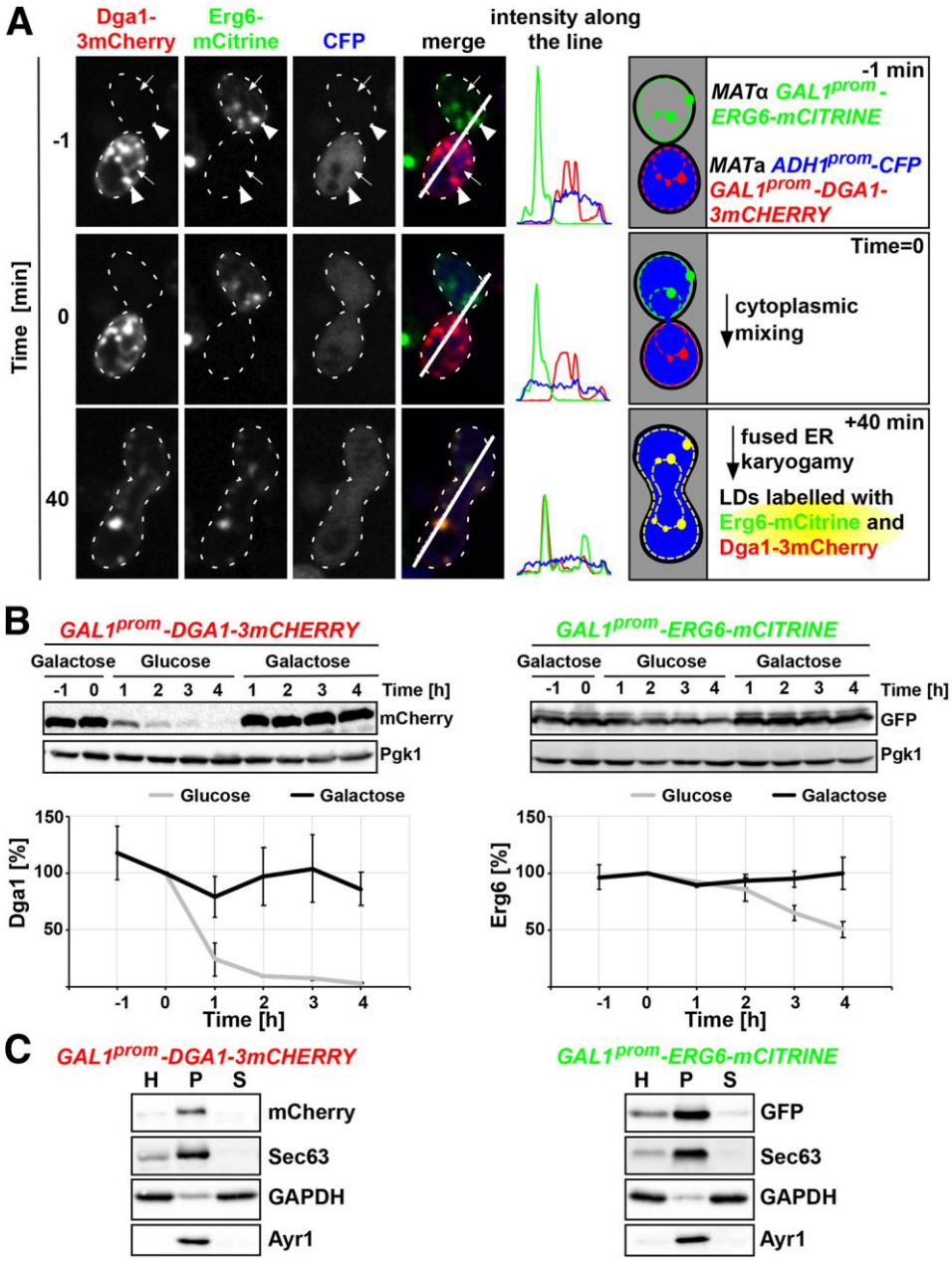

Figure 1. Experimental design to monitor the exchange of LD proteins upon cell fusion.

(A) A yeast mating-based assay to follow the exchange of LD-localized proteins. *MAT*a cells co-expressing Dga1-3mCherry *(GAL1^{prom}-DGA1-3mCHERRY)* with a soluble cytosolic CFP (*ADH1^{prom}-CFP)* and *MAT*α cells expressing Erg6-mCitrine *(GAL1^{prom}-ERG6-mCITRINE)* were grown in galactose supplemented media to induce

expression of the markers. Cells were then mixed in a 1:1 ratio and shifted to glucose medium for 2 h before imaging. Cells were collected, mounted on a glass slide and covered with an agarose patch to allow live cell imaging over an extended period of time. Time 0 of the mating event was defined as the time point of cytoplasmic mixing, monitored by the dispersion of CFP into the newly formed zygote. Shown are single confocal sections for each of the three fluorophores 1 min before (t=-1), at the time of cytoplasmic mixing (t=0), and 40 min after cell fusion had occurred. The fluorescence intensity profile along the white line shown in the merge is plotted. Colocalization of the two LD markers, Dga1-3mCherry and Erg6-mCitrine is indicated by yellow in the merge. A schematic illustration of the mating event and transfer of marker proteins is shown to the right. Arrows point to the ER membrane, arrowheads to LDs. Scale bar, 5 µm.

(B) Turnover of Dga1-3mCherry and Erg6-mCitrine upon glucose repression. Cells expressing the LD marker proteins Dga1-3mCherry or Erg6-mCitrine under control of a galactose inducible promoter (*GAL1*^{prom}) were cultivated in galactose-containing media and then shifted into fresh media containing either glucose or galactose, samples were taken every hour and protein levels were analyzed by Western blotting using the constitutively expressed 3-phosphoglycerate kinase (Pgk1) as loading standard. Protein levels, normalized to t=0, are plotted in the graphs. Values represent mean ± SD of 3 independent experiments.

(C) The LD marker proteins Dga1-3mCherry and Erg6-mCitrine are membrane associated. The fractionation properties of Dga1-3mCherry and Erg6-mCitrine was assessed by differential centrifugation. Equal amounts of proteins from the cell homogenate (H), the membrane pellet fraction (P, 30’000 g), and the soluble supernatant (S) were separated by SDS-PAGE and probed with antibodies against mCherry, GFP, the soluble glyceraldehyde-3-phosphate dehydrogenase (GAPDH), the LD resident protein Ayr1, or Sec63, a component of the ER translocon.

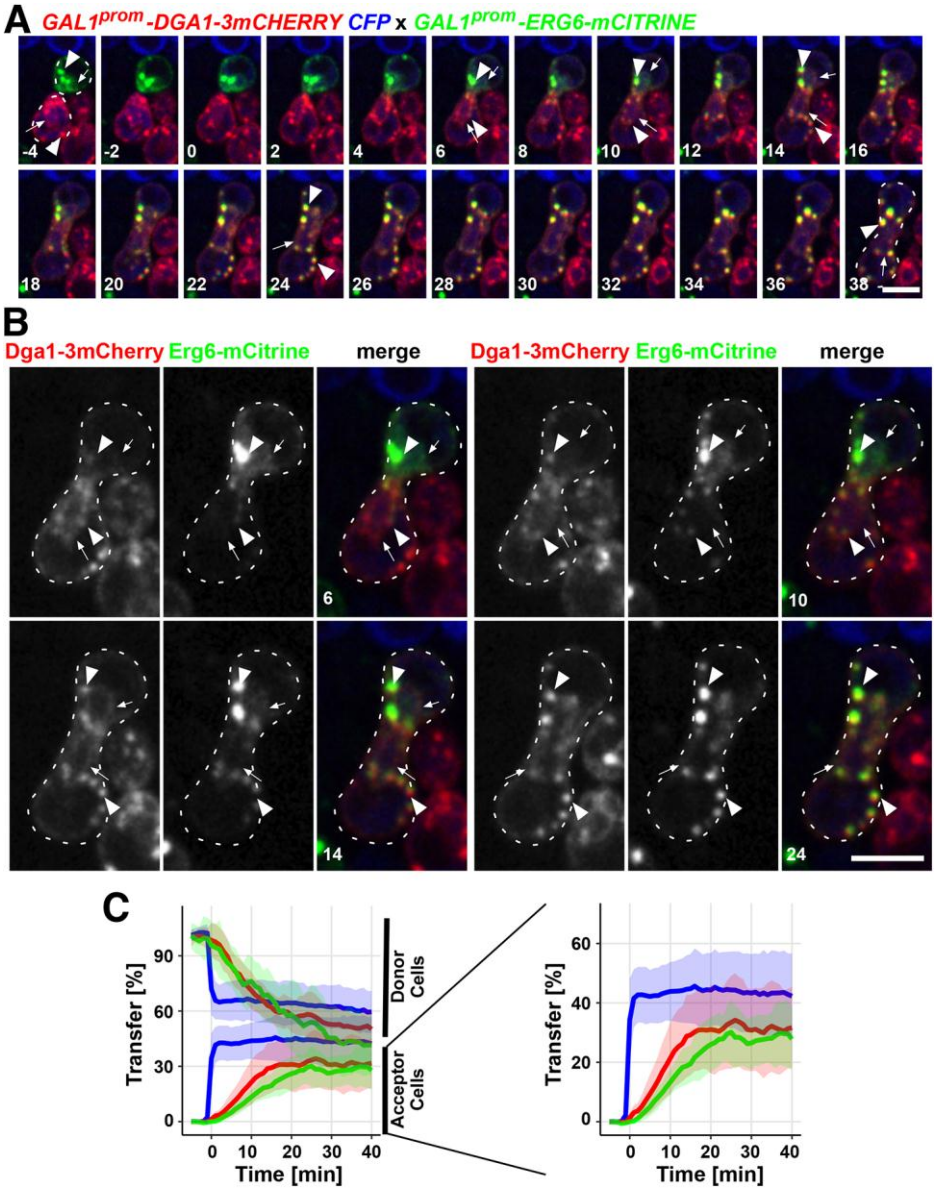

Figure 2. Exchange of proteins between LDs of mating partners is continuous, reciprocal, and occurs on many LDs concurrently.

(A) Exchange of LD proteins between mating partners. Representative time-lapse images showing the transfer of Dga1-3mCherry and Erg6-mCitrine into the mating partner. Images were acquired every 1 min, but only even time points are depicted starting 4 min before cytoplasmic mixing as monitored by spreading of the soluble CFP into the fusion partner (t=0). Arrows point to the ER membrane, arrowheads to LDs. Scale bar, 5 µm.

(B) Enlarged views of the 6, 10, 14, and 24 min time points shown in panel A. Note the simultaneous and uniform acquisition of Erg6-mCitrine on multiple LDs

containing Dga1-3mCherry, and *vice versa*. Arrows point to the ER membrane, arrowheads to LDs. Scale bar, 5 µm.

(C) The exchange of LD proteins into the mating partner occurs through a continuous and reciprocal process. The graph shows the time-dependent decrease (upper part) and increase (lower part) in fluorescence in the mating partners. Transfer of Dga1-mCherry is indicated by the red lines, that of Erg6-mCitrine by the green lines. The fast re-distribution of CFP fluorescence upon cytoplasmic mixing at t=0 is shown by the blue lines. The increase in fluorescence in the acceptor cells is enlarged in the graph to the right. Values represent mean ± SD of 10 individual mating events.

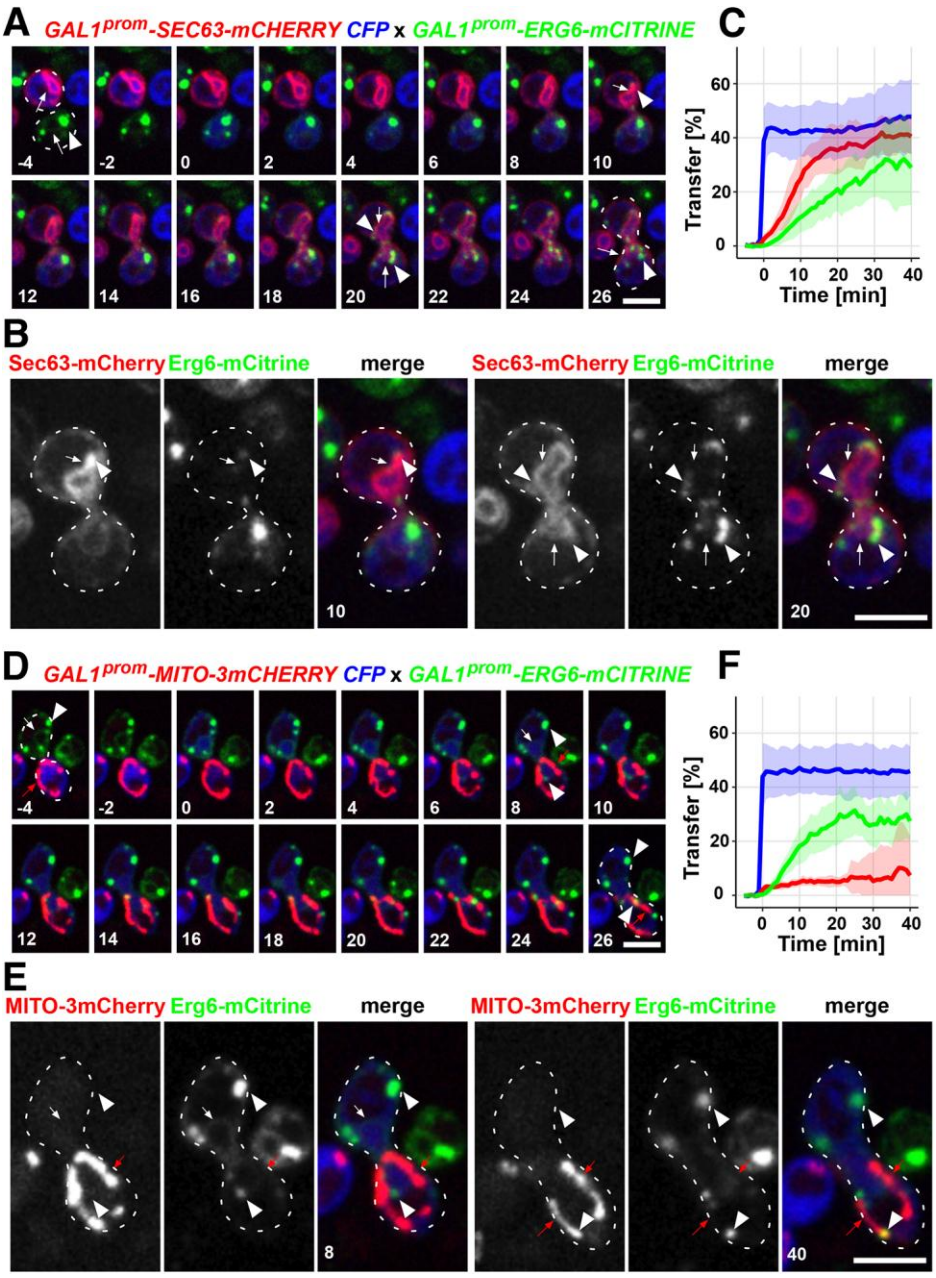

Figure 3. Comparison of the transfer of LD proteins to that of the ER protein Sec63 and to a mitochondrial marker.

(A, D) Comparison of transfer of proteins localized to LDs, the ER membrane, or mitochondria into the mating partner. Representative time-lapse images showing the transfer of the ER translocon component Sec63-mCherry (A), or the mitochondrial marker MITO-3mCherry (D) into the mating partner expressing the LD marker Erg6-mCitrine. Images were acquired every 1 min, but only even time points are depicted starting 4 min before cytoplasmic mixing, as monitored by spreading of the soluble

CFP into the fusion partner (t=0). White arrows point to the ER membrane, red arrows to mitochondria, and arrowheads to LDs. Scale bar, 5 µm.

(B, E) Enlarged views of the 10 and 20 min time points shown in panel A (B) and of the 8 and 40 min time points after cytoplasmic mixing represented in panel D (E). Note the close apposition of Erg6-mCitrine to the ER (B). White arrows point to the ER membrane, red arrows to mitochondria, and arrowheads to LDs. Scale bar, 5 µm.

(C, F) The graphs show the time-dependent increase in fluorescence in the mating partners. Transfer of Sec63-mCherry (C) and MITO-3mCherry (F), respectively, is indicated by the red lines. Transfer of Erg6-mCitrine onto acceptor LDs is indicated by the green lines. The fast increase in CFP fluorescence upon cytoplasmic mixing at t=0 is shown by the blue lines. Note that MITO-3mCherry is not transferred continuously to the mating partner, as is Sec63-mCherry or Erg6-mCitrine. Values represent mean ± SD of 10 mating events.

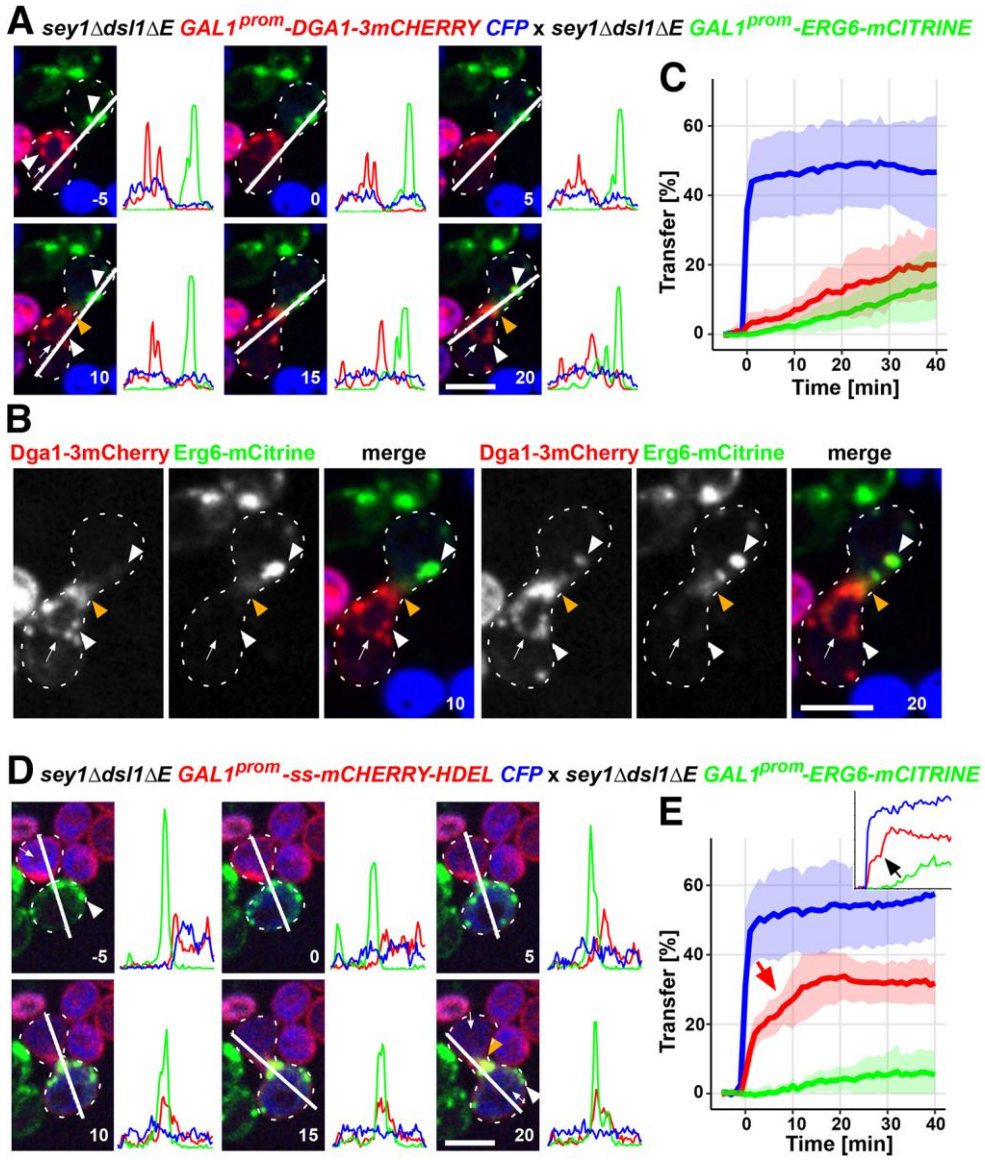

Figure 4. Transfer of LD proteins between mating partners in mutants with defects in ER fusion.

(A) Time-lapse images of mating reactions to monitor the exchange of Dga1-mCherry and Erg6-mCitrine between mutant cells having defects in ER fusion (*sey1*Δ *dsl1*Δ*E*). Images shown are separated by 5 min intervals over a period of 25 min, starting 5 min (t=-5) before cytoplasmic mixing (t=0), but mating progression was recorded every minute. Fluorescence intensity profiles along the white line crossing through the mating partners are plotted. Arrows point to the ER membrane, arrowheads to LDs. Scale bar, 5 µm.

(B) Enlarged views of the mating reaction after 10 min and 20 min of cytoplasmic mixing, respectively. Arrows point to the ER membrane, white arrowheads to LDs,

and orange arrowheads to membrane accumulation at the fusion neck. Scale bar, 5 µm.

(C) The transfers of the marker proteins between the mating cells are plotted in the graph. The red line represents Dga1-3mCherry, the green line represents Erg6-mCitrine, and the blue line represent CFP. Values represent mean ± SD of 10 individual mating events with data acquired at 1 min intervals.

(D) Transfer of the ER luminal ss-mCherry-HDEL and Erg6-mCitrine between *sey1*Δ *dsl1*Δ*E* mating partners. Imaging conditions were as described for panel A. Arrows point to the ER membrane, white arrowheads to LDs, and the orange arrowheads to membrane accumulation at the fusion neck. Scale bar, 5 µm.

(E) The rates of transfer of ss-mCherry-HDEL between *sey1*Δ *dsl1*Δ*E* mutant partners. The red line corresponds to ss-mCherry-HDEL, the green line to Erg6-mCitrine, and CFP is represented by the blue line. The red arrow points to the flattening of the average transfer curve of ss-mCherry-HDEL, indicating a delay in ER fusion. This delay, followed by a sharp increase, is more apparent in single mating events, as shown in the inlet and indicated by a black arrow. Values represent mean ± SD of 10 individual mating events with data acquired at 1 min intervals.

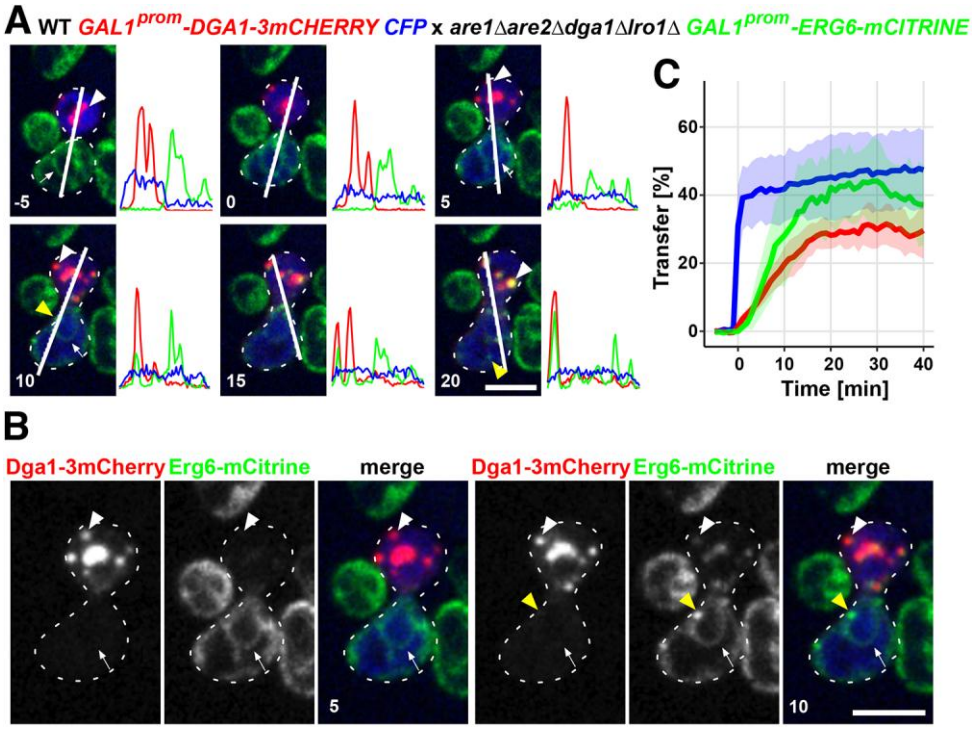

Figure 5. Transfer of an LD protein from the ER of a donor cell to LDs of an acceptor mating partner.

(A) Time-lapse images of mating reactions to monitor the dynamics of Erg6-mCitrine located in the ER of a mutant cell lacking LDs (*4*Δ, *are1*Δ *are2*Δ *dga1*Δ *lro1*Δ) and Dga1-3mCherry labelling of LDs in a wild-type strain (WT). Images shown are separated by 5 min intervals over a period of 25 min, starting 5 min (t=-5) before cytoplasmic mixing (t=0). Fluorescence profiles along the white line crossing through the mating partners are plotted. The ER membrane is highlighted by arrows, arrowheads point to LDs, white for the LDs in the WT cell, and yellow for LDs that appears to form in the *4*Δ mutant. Scale bar, 5 µm.

(B) Enlarged views of the mating reaction at 5 min and 10 min after cytoplasmic mixing. Arrows point to the ER membrane, arrowheads to LDs, the yellow arrowheads point to an LD that appears to form in the ER of the *4*Δ mutant mating partner. Scale bar, 5 μm.

(C) The rate of transfer of the marker proteins between the mating cells is plotted in the graph. The red line represents Dga1-3mCherry, the green line represents Erg6-mCitrine, and the blue line represents CFP. Values represent mean ± SD of 10 individual mating events with data acquired at 1 min intervals.

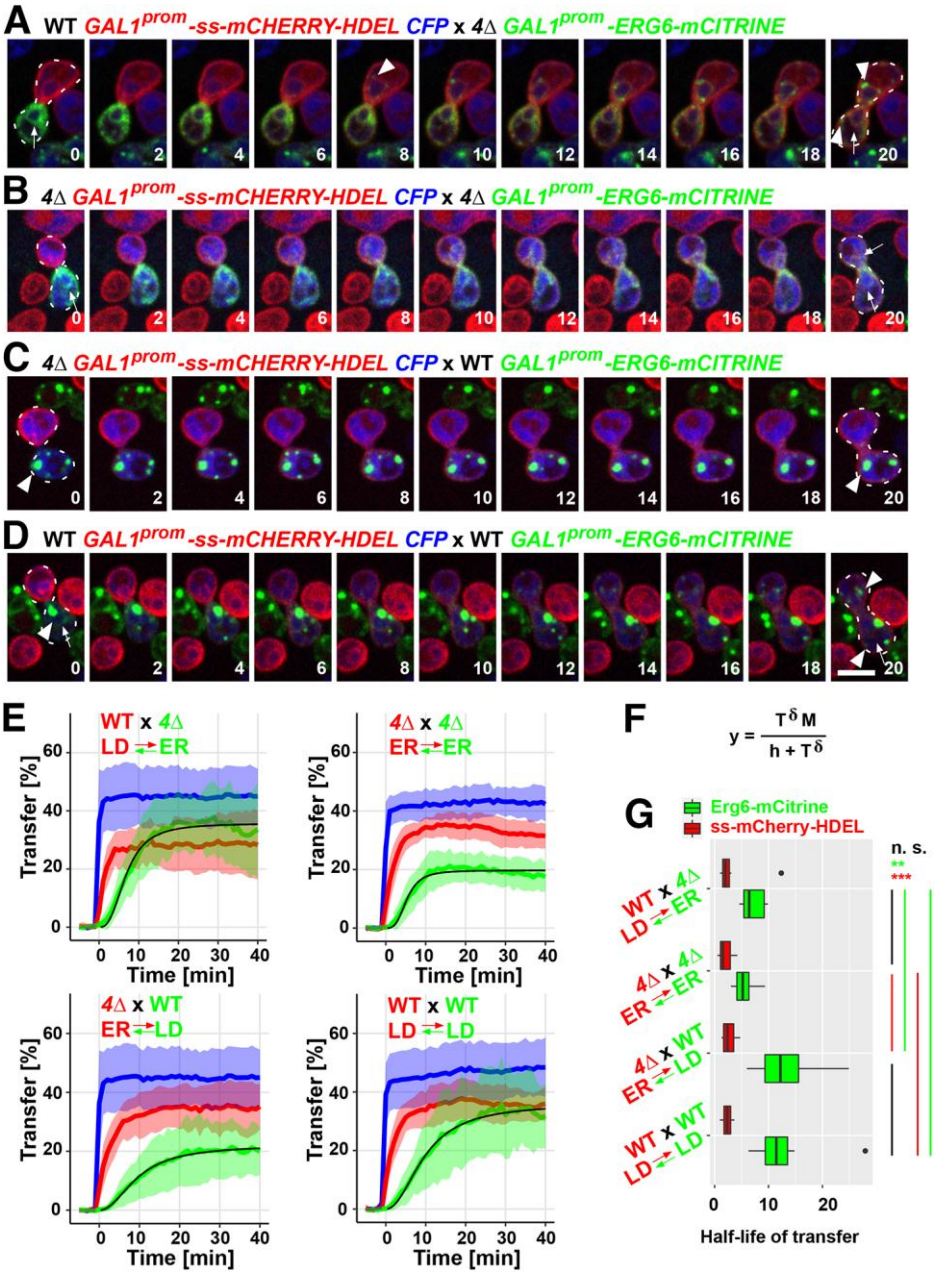

Figure 6. Comparison between the rates with which proteins associate and dissociate from LDs.

(A-D) Time-lapse images of mating reactions to monitor the exchange of the ER luminal marker ss-mCherry-HDEL and Erg6-mCitrine between wild-type (WT) cells containing LDs or mutant cells lacking LDs (*4Δ, are1Δ are2Δ dga1Δ lro1Δ*). Images were recorded at 1 min intervals over a period of 20 min from the time of cytoplasmic mixing (t=0). Images shown represent 2 min intervals. Arrows point to the ER membrane, arrowheads to LDs. Scale bar, 5 µm.

(E) The rates of transfer of marker proteins between mating partners of the indicated genotypes are plotted in the graphs. Red lines represent ss-mCherry-HDEL, green lines represent Erg6-mCitrine and blue lines represent CFP. Fitting of the rate of transfer of Erg6-mCitrine to the Hill equation is indicated by the thin black line. Values represent mean ± SD of 9 different mating events with data acquired at 1 min intervals.

(F) Hill equation where T = time, M = maximal fluorescence intensity, $h = ½T^{\boldsymbol{\delta}}$, $\boldsymbol{\delta}$ = slope of the curve.

(G) The median half-life of transfer ($h^{(1/\boldsymbol{\delta})}$) of Erg6-mCitrine (green) and ss-mCherry-HDEL (red) was calculated by fitting transfer curves to individual mating events and analyzing the data in a box plot. The box represents the 25-75th percentile range and the median is indicated. The whiskers denote maximum and minimum values, outliers are depicted by black circles. Difference between the median half-life of the transfer of ss-mCherry-HDEL from the donor ER to the recipient ER are statistically non-significant, as indicated by a Kruskal-Wallis p-value of 0.52. On the other hand, the p-value for the median half-life of transfer of Erg6-mCitrine between the ER and LDs is 0.0001, indicating that these differences are significant. Therefore, for this data set, the statistical significance between the different mating combinations was calculated by a pairwise comparisons using the Wilcoxon rank-sum test. n.s., none significant (black); **p-value < 0.01 (green); ***p-value < 0.001 (red); n > 9 individual mating events.

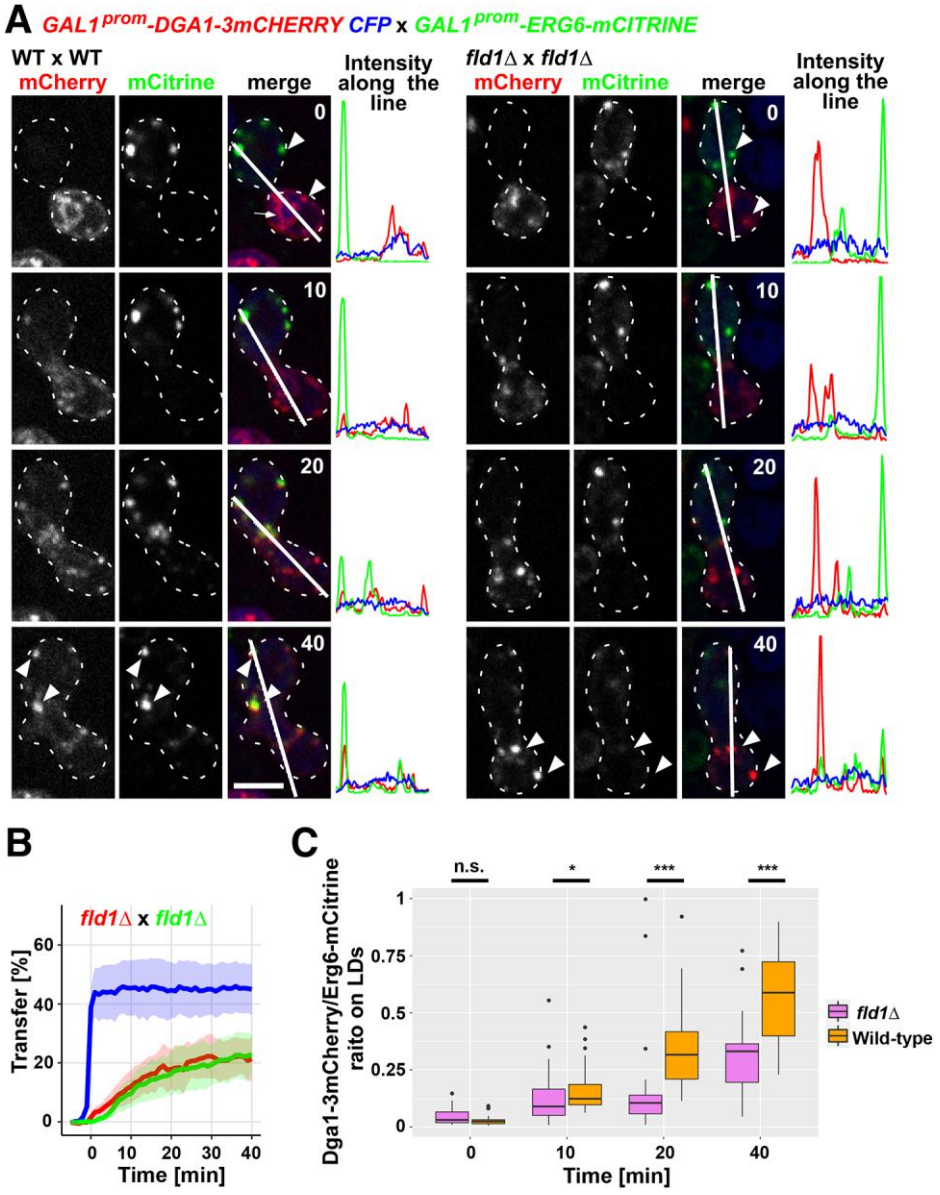

Figure 7. Seipin is required for efficient targeting of proteins to LDs.

(A) Time-lapse images showing the exchange of the LD proteins Dga1-3mCherry and Erg6-mCitrine between wild-type cells (WT, left panels) and seipin mutant cells (*fld1*Δ, right panels). Images shown were acquired at time of cytoplasmic mixing (t=0 min), and after 10, 20, and 40 min. Fluorescence intensity profiles along the white line crossing through LDs of both mating partners are plotted to the right of the merge. Red lines represent Dga1-3mCherry, green lines represent Erg6-mCitrine, and blue lines show CFP fluorescence. Arrows point to the ER membrane, arrowheads to LDs. Note that the white arrowheads at the 40 min time point indicate LDs with similar ratios of the two marker proteins in WT cells, but differences in marker protein composition in seipin mutant diploids. Scale bar, 5 µm.

(B) Rate of transfer of Dga1-3mCherry and Erg6-mCitrine between seipin mutant *(fld1Δ)* cells. Same color code as in (A). Values represent mean ± SD of 10 individual mating events with data acquired at 1 min intervals.

(C) The relative fluorescence of Dga1-3mCherry on Erg6-mCitrine labelled LDs is shown in the box plot. The box represents the 25-75th percentiles, the median is indicated by the solid line, and the whiskers denote maximum and minimum, outliers are represented by black circles. Wild-type data are shown in orange, *fld1*Δ in pink. Statistical significance was scored with the Wilcoxon rank-sum test (n > 19 LDs). n.s., not significant; *p-value < 0.05; ***p-value < 0.001;.

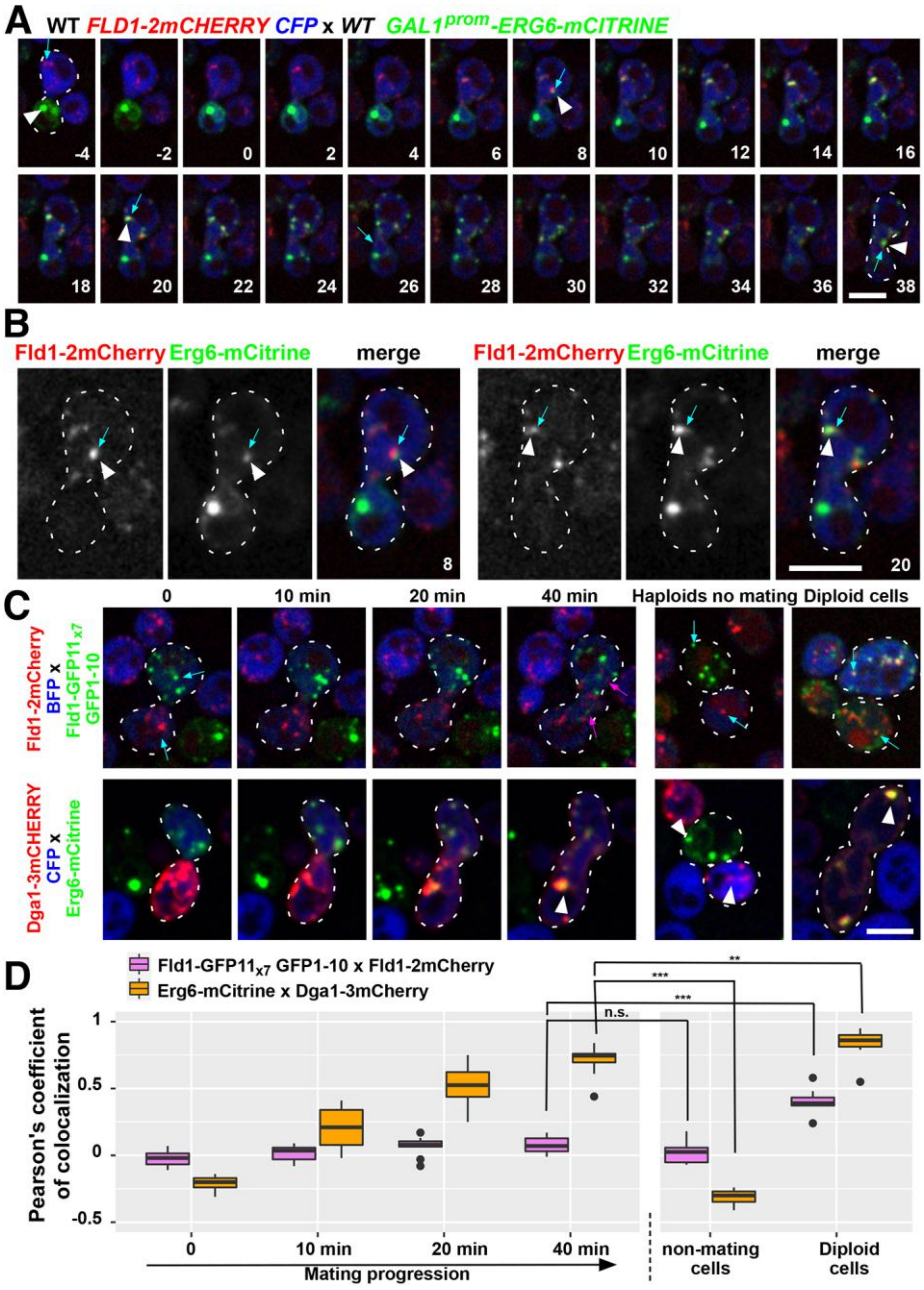

Figure 8. Seipin is required for efficient targeting of proteins to LDs.

(A) Erg6-mCitrine accumulates in the mating partner at ER sites marked by seipin. Representative time-lapse images showing the transfer of Erg6-mCitrine into a mating partner expressing a 2mCherry-tagged seipin, Fld1-2mCherry. Images shown were recorded at 2 min intervals, starting 4 min (t=-4) before cytoplasmic mixing (t=0), over a period of 42 min. Blue arrows point to the seipin/Fld1 spots, arrowheads to LDs. Scale bar, 5 µm.

(B) Enlarged views of the 8 and 20 min time points shown in panel A. Blue arrows point to the seipin/Fld1 spots, arrowheads to LDs. Scale bar, 5 µm.

(C) Seipin domains are stable and do not mix. Representative time-lapse images to monitor the transfer of Fld1-2mCherry and Fld1-GFP11$_{x7}$ GFP1-10 (upper row) or that of Dga1-3mCherry and Erg6-mCitrine (bottom row) upon zygote formation, at 0, 10, 20, and 40 min of cytoplasmic mixing. The same combination of proteins was also imaged in non-mating haploid cells and in diploids. Note the colocalization of mCherry- and GFP-tagged seipin when both variants are simultaneously expressed in diploid cells. Blue arrows point to seipin spots, lila arrows point to seipin spots that have moved into the mating partner at the 40 min time point, white arrow heads point to LDs. Scale bar, 5 μm.

(D) Upon mating Fld1 tagged proteins do not merge as LD marker proteins do. Boxplot representing Pearson correlation coefficients of colocalization between mCherry- and GFP-tagged seipin variants (Fld1-2mCherry and Fld1-GFP11$_{x7}$ GFP1-10; pink boxes), and between the LD markers Dga1-3mCherry and Erg6-mCitrine (orange boxes), upon progression of zygote formation, i.e., after 0, 10, 20, and 40 min of cytoplasmic mixing. The same analysis is shown for haploid non-mating cells and for diploid cells expressing both fluorophores simultaneously. The median is indicated within a box that represents the 25-75th percentile range. The whiskers denote maximum and minimum values, outliers are depicted by black circles. Statistical significance was scored with the Wilcoxon rank-sum test. n.s., not significant; **p-value < 0.01; ***p-value < 0.001; n = 10 mating events, or cells.

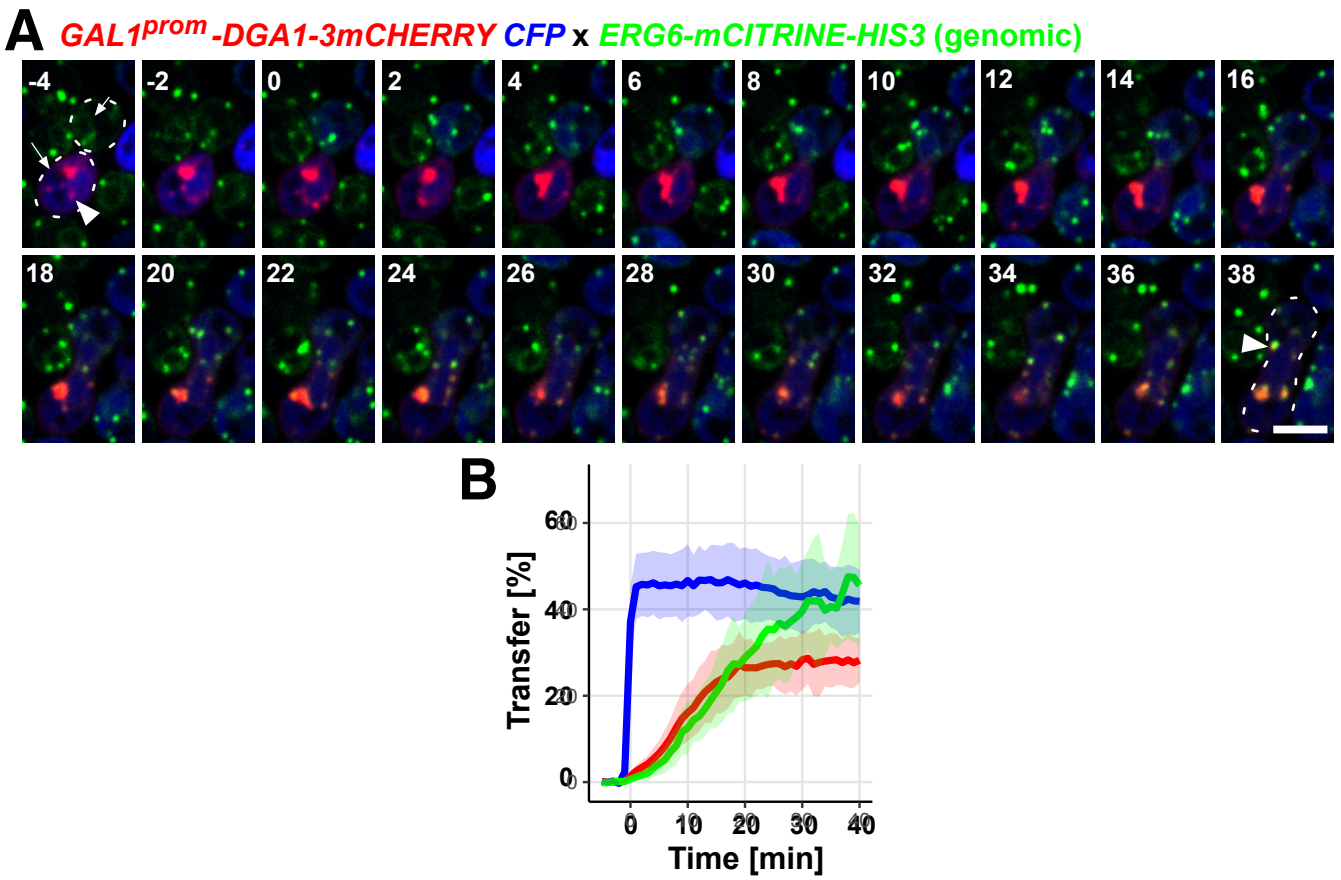

Fig. S1. Transfer of endogenous mCitrine-tagged Erg6 to LDs of the mating partner, and movement of Pet10-mScarlet labelled LDs on zygote formation.

(A) Mating reactions to monitor the exchange of endogenously tagged Erg6-mCitrine and of Dga1-3mCherry, whose expression is control by a galactose inducible promoter, in wild-type cells. Time-lapse images shown are separated by 2 min intervals over a period of 44 min, starting 2 min prior to cytoplasmic mixing (t=0 min). White arrows point to the ER membrane, and arrowheads to LDs. Scale bar, 5 µm.

(B) Rate of transfer of Erg6-mCitrine (green line), Dga1-3mCherry (red line), and the cytosolic marker CFP (blue line) between wild-type mating partners.

(C) Pet10-mScarlet labelled LDs move only slowly into the acceptor half of the zygote upon cytoplasmic mixing. Representative time-lapse images showing the transfer of Pet10-mScarlet and Erg6-mCitrine onto the LDs of mating partners. Images shown are separated by 2 min intervals, starting 4 min (t=-4) before cytoplasmic mixing (t=0), over a period of 42 min. White arrowheads point to LDs, and the red arrowhead marks an LD that has moved into the mating partner. Scale bar, 5 µm.

(D) Enlarged views of the 14 and 34 min time points shown in panel C. White arrowheads point to LDs that are still in the part of the zygote where they originate from, and the red arrowhead points to an LD that is strongly labelled with Pet10-mScarlet and that has moved into the mating partner more than 30 min after fusion had occurred. Scale bar, 5 µm.

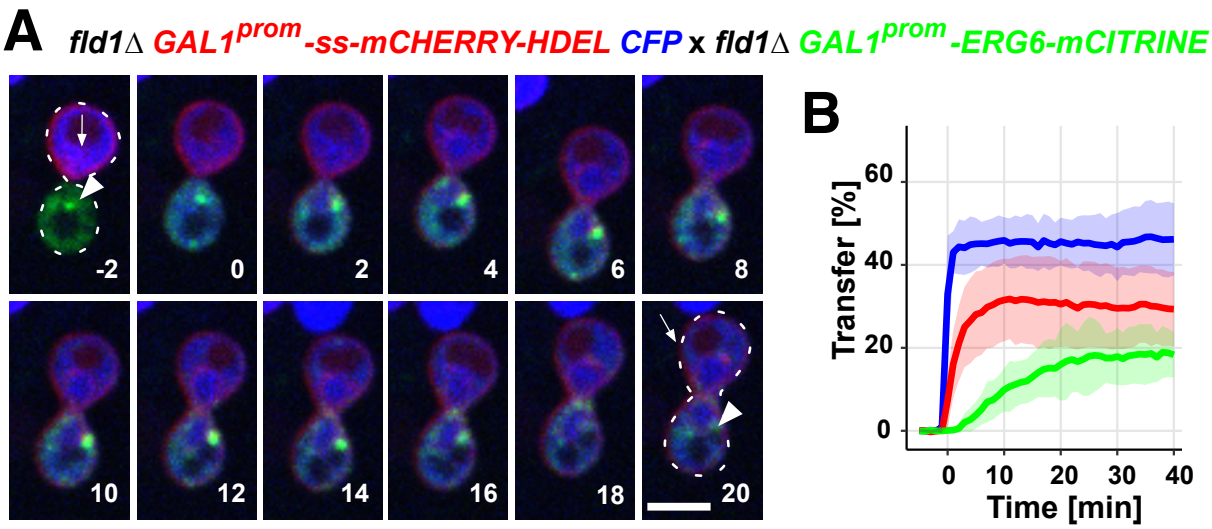

Fig. S2. Seipin affects the exchange of LD proteins but not ER fusion.

(A) Mating reactions to monitor the exchange of ss-mCherry-HDEL and Erg6-mCitrine between seipin (*fld1*Δ) mutant cells. Time-lapse images shown are separated by 2 min intervals over a period of 22 min, starting 2 min prior to cytoplasmic mixing (t=0 min). Arrows point to the ER membrane, arrowheads to LDs. Scale bar, 5 µm.

(B) Rate of transfer of the ER luminal marker ss-mCherry-HDEL and that of the LD marker Erg6-mCitrine between seipin mutant *(fld1*Δ*)* cells. The red line represents ss-mCherry-HDEL, the green line Erg6-mCitrine, and the blue line cytosolic CFP.

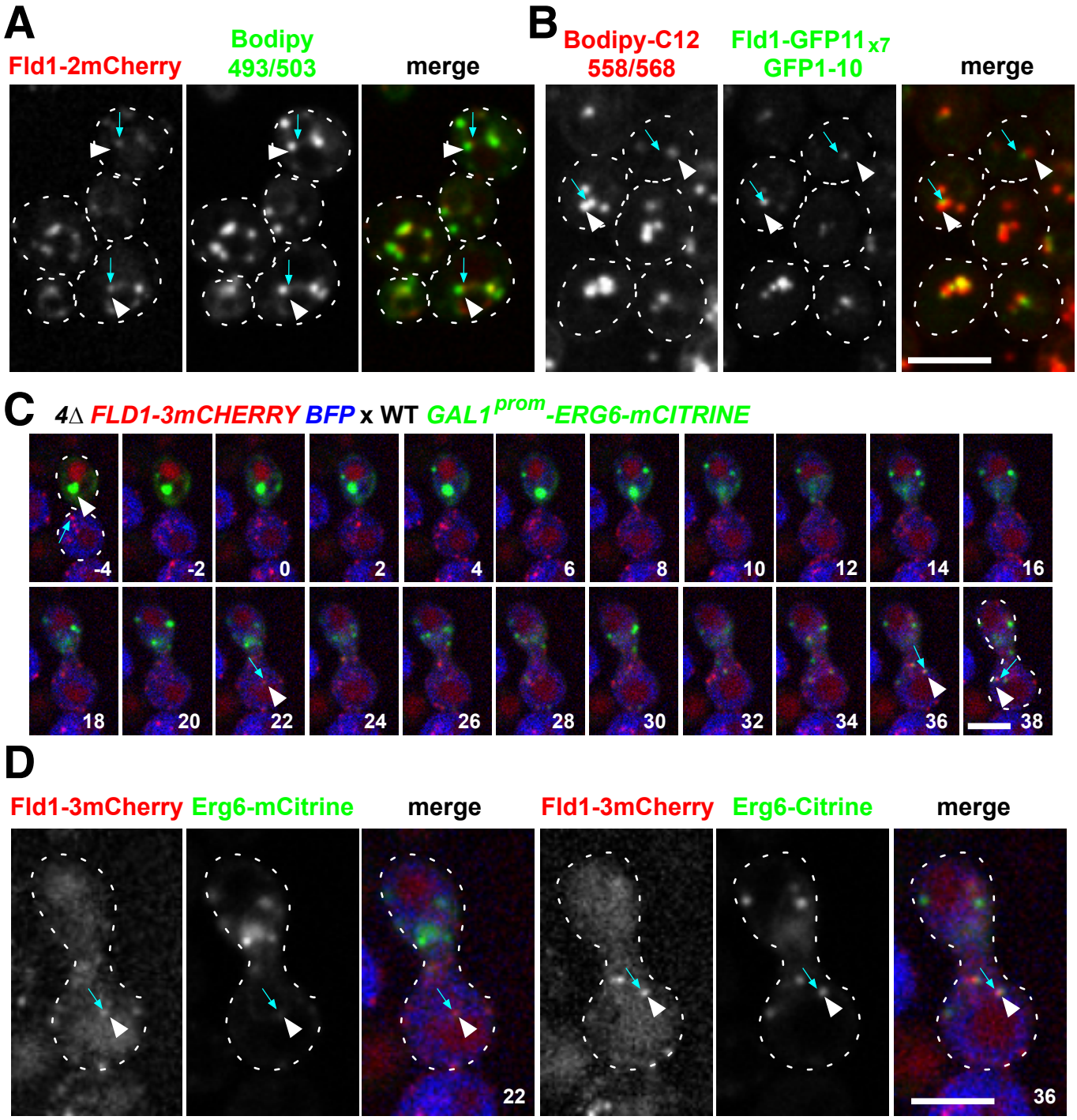

Fig. S3. mCherry- and GFP-tagged variants of seipin are functional and mark sites of LD formation.

(A, B) 2mCherry- and the split-GFP- (sfGFP11$_{x7}$+GFP1-10) tagged Fld1 localize at the base of LDs labelled with either BODIPY493/503 (panel A) or BODIPY-C12 (558/568) (panel B), respectively. Blue arrows point to Fld1 spots, arrowheads to LDs. Scale bar, 5 µm.

(C) Fld1-3mCherry marks sites of LD formation in the ER of quadruple mutant cells. Wild-type cells expressing Erg6-mCitrine were mated to quadruple mutant cells, *4*Δ (*are1*Δ *are2*Δ *dga1*Δ *lro1*Δ) expressing Fld1-3mCherry. Images shown were recorded at 2 min intervals, starting 4 min (t=-4) before cytoplasmic mixing (t=0) over a period of 42 min. Blue arrows point to Fld1 spots, arrowheads to LDs. Scale bar, 5 µm.

(D) Enlarged views of the 22, and 36 min time points shown in panel A. Note the accumulation of Erg6-mCitrine at ER spots marked by Fld1-3mCherry. Blue arrows point to Fld1 spots, arrowheads to LDs. Scale bar, 5 µm.

Table S1. *Saccharomyces cerevisiae* strains used in this study

Strain	Genotype	Source	Figure
BY4741	*MAT*a; *his3Δ1 leu2Δ met15Δ0 ura3Δ0*	Euroscarf	1, 2, 3, 5, 6, 7
BY4742	*MAT*α; *his3Δ1 leu2Δ0 lys2Δ0 ura3Δ0*	Euroscarf	1, 2, 3, 6, 7, 8
RSY5669	*MAT*α; *his3Δ1 leu2Δ0 lys2Δ0 ura3Δ0 are1Δ::KanMX4 are2Δ::KanMX4 dga1Δ::KanMX4 lro1Δ::KanMX4*	This study	5, 6
RSY5795	*MAT*a; *his3Δ1 leu2Δ0 lys2Δ0 ura3Δ0 are1Δ::KanMX4 are2Δ::KanMX4 dga1Δ::KanMX4 lro1Δ::KanMX4*	This study	6
MATa thr$^-$	*MAT*a; *thr*	Lab collection	
MATα thr$^-$	*MAT*α; *thr*	Lab collection	
MY14769	*MAT*a/α; *his3Δ1/his3Δ1 leu2Δ0/leu2Δ0 met15Δ0/met15Δ0 ura3Δ0/ura3Δ0 sey1Δ::Hyg/SEY1 yop1Δ::URA3/YOP1 dsl1ΔE-NatMX/DSL1*	Mark Rose	
RSY5619	*MAT*α; *his3Δ1 leu2Δ0 met15Δ0 ura3Δ0 sey1Δ::Hyg dsl1ΔE-NatMX*	This study	4
RSY5621	*MAT*a; *his3Δ1 leu2Δ0 met15Δ0 ura3Δ0 sey1Δ::Hyg dsl1ΔE-NatMX*	This study	4
MATa fld1Δ	*MAT*a; *his3Δ1 leu2Δ met15Δ0 ura3Δ0 fld1Δ::KanMX4*	Euroscarf	7, S2
MATα fld1Δ	*MAT*α; *his3Δ1 leu2Δ0 lys2Δ0 ura3Δ0 fld1Δ::KanMX4*	Euroscarf	7, S2
RSY6911	*MAT*α; *his3Δ1 leu2Δ lys2Δ0 ura3Δ0 FLD1-2mCHERRY::SpHIS5*	This study	8, S2
RSY6970	*MAT*a; *his3Δ1 leu2Δ met15Δ0 ura3Δ FLD1-GFP11x7::SpHIS5*	This study	8, S3
RSY6963	*MAT*α; *his3Δ1 leu2Δ0 lys2Δ0 ura3Δ0 are1Δ::KanMX4 are2Δ::KanMX4 dga1Δ::KanMX4 lro1Δ::KanMX4 FLD1-3mCHERRY::SpHIS5*	This study	S3
RSY6756	*MAT*α; *his3Δ1 leu2Δ0 lys2Δ0 ura3Δ0 ERG6-mCITRINE::SpHIS5*	This study	S1

Table S2. Plasmids used in this study

Plasmids	Genotype	Source	Figure
pRS415-ADH1	*CEN/ARS, ADH1^{prom}, LEU2*	Mumberg et al., 1995	
p1174	[pRS415] *ADH1^{prom}-yECFP*	Cottier et al., 2020	1, 2, 3, 4, 5, 6, 7, 8, S1, S2
pGREG506	*CEN/ARS, GAL1^{prom}, URA3*	Jansen et al., 2005	
pKT211	[pFA6a] *link-yEmCITRINE, SpHIS5*	Sheff and Thorn, 2004	
p1307	[pGREG506] *GAL1^{prom}-ERG6-mCITRINE^{A206K}*	This study	1, 2, 3, 4, 5, 6, 7, 8, S2, S3
p30648	*POM121-3mCHERRY*	Dultz and Ellenberg, 2010	
pGREG600	*CEN/ARS, GAL1^{prom}-RecombinationSite-GFP, URA3*	Jansen et al., 2005	
p1079	[pGREG600] *GAL1^{prom}-RecombinationSite-3mCHERRY*	This study	
p1102	[p1079] *GAL1^{prom}-DGA1-3mCHERRY*	This study	1, 2, 4, 5, 7, S1
Mito-RFP	*CEN/ARS NcATP9$^{mitochondria\text{-}signal}$-RFP, LEU2*	Westermann and Neupert, 2000	
p1317	[p1079] *GAL1^{prom}- NcATP9$^{mitochondria\text{-}signal}$-3mCHERRY*	This study	3
p1312	[p1079] *GAL1^{prom}-SEC63-3mCHERRY*	This study	3
pGREG503	*CEN/ARS, GAL1^{prom}, HIS3*	Jansen et al., 2005	
MR6474	*CEN, ADH1^{prom}-PRC1^{ss}-mCHERRY-HDEL, LEU2*	Rogers et al., 2014	
p1171	[pGREG503] *GAL1^{prom}-PRC1^{ss}-mCHERRY-HDEL*	This study	4, 6, S2
pGAL-HO	*GAL^{prom}-HO-URA*	Herskowitz and Jensen, 1991	
Addgene #70224	*pHRm-NLS-dCas9-GFP11x7-NLS*	Kamiyama et al., 2016	
Addgene #129416	*pSH-EFIRES-P-GFP(1-10)opti*	Salo et al., 2019	
pRS416-ADH1	*CEN/ARS, ADH1^{prom}, LEU2*	Mumberg et al., 1995	
p2213	[pRS416] *ADH1^{prom}-sfGFP1-10*	This study	8, S3
p2216	[pRS415] *ADH1^{prom}-BFP*	This study	8, S3
p2233	[pRS415] *GAL1^{prom}-ERG6-mCITRINE*	This study	8
P1662	[pRS416] *GAL1^{prom}-PET10-mSCARLET*	This study	S1
pKT175	[pFA6a] *link-yECITRINE, CaURA3*	Sheff and Thorn, 200	

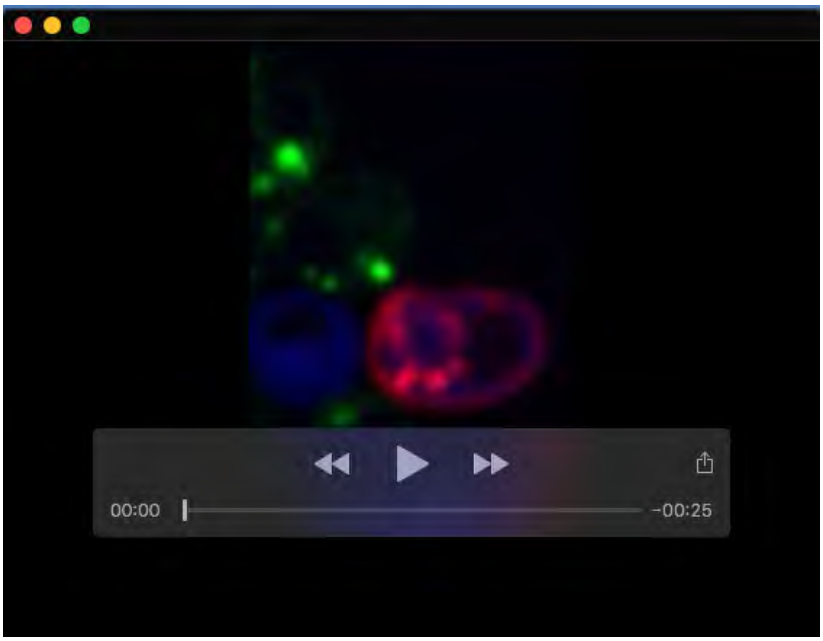

Movie 1. Redistribution of LD markers upon zygote formation.

Time-lapse images during zygote formation between a *MAT*a cell expressing Dga1- 3mCherry and CFP and a *MAT*α cell expressing Erg6-mCitrine. Expression of the LD marker proteins under control of a galactose inducible promoter was repressed by shifting cells to glucose media 2 h before imaging. Single-plane images were recorded at 1 min intervals.

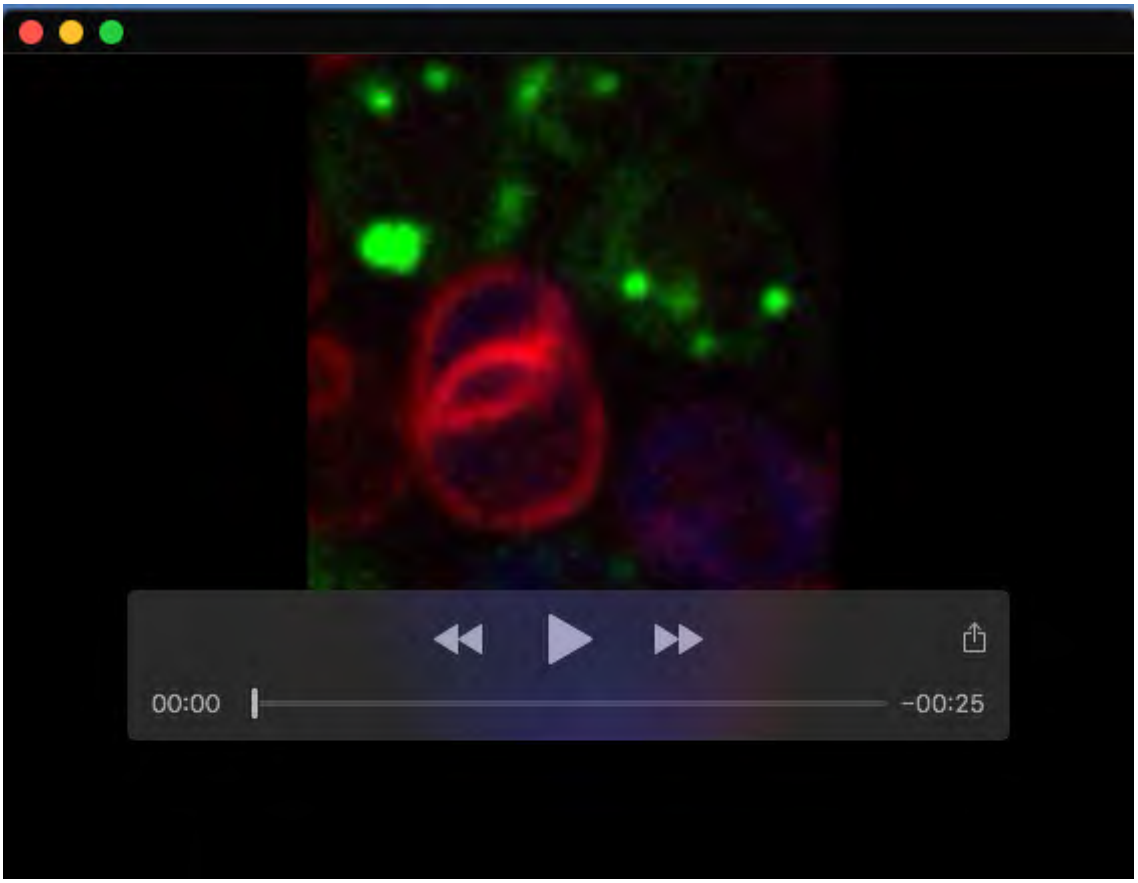

Movie 2. Redistribution of the ER marker Sec63-mCherry and the LD marker Erg6-mCitrine upon zygote formation.

Time-lapse images of zygote formation between a *MAT*a cell expressing Sec63-mCherry and CFP and *MAT*α cell expressing Erg6-mCitrine. Expression of Sec63-mCherry and Erg6-mCitrine was switched off 2 h before imaging by shifting cells to glucose medium. Single-plane images were recorded at 1 min intervals.

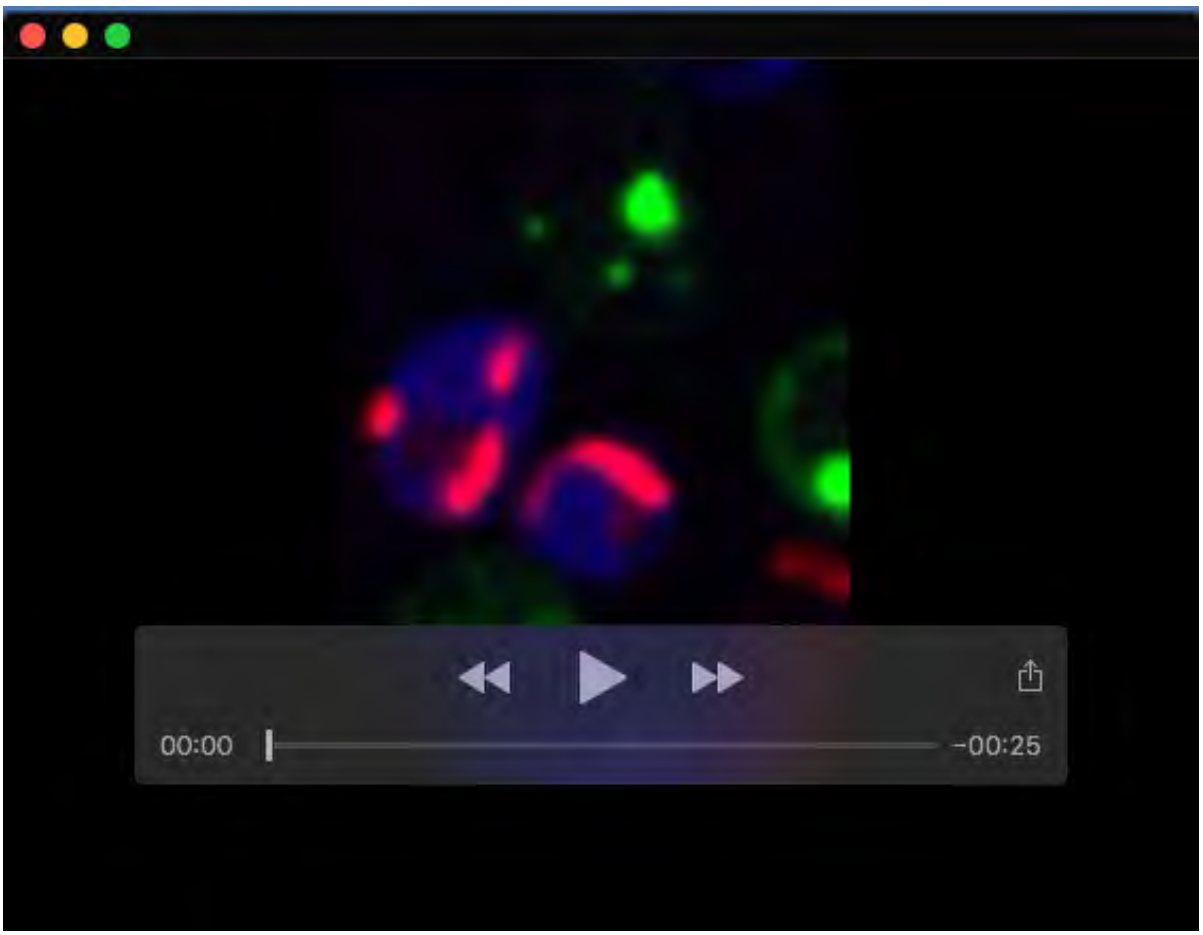

Movie 3. Dynamics of exchange of the LD marker Erg6-mCitrine and the mitochondrial matrix marker MITO-3mCherry upon zygote formation.

Time-lapse images of zygote formation between a *MAT*a cell expressing MITO-3mCherry and CFP and a *MAT*α cell expressing Erg6-mCitrine. Expression of MITO-3mCherry and Erg6-mCitrine was switched off 2 h before imaging by shifting cells to glucose medium. Single-plane images were recorded at 1 min intervals.

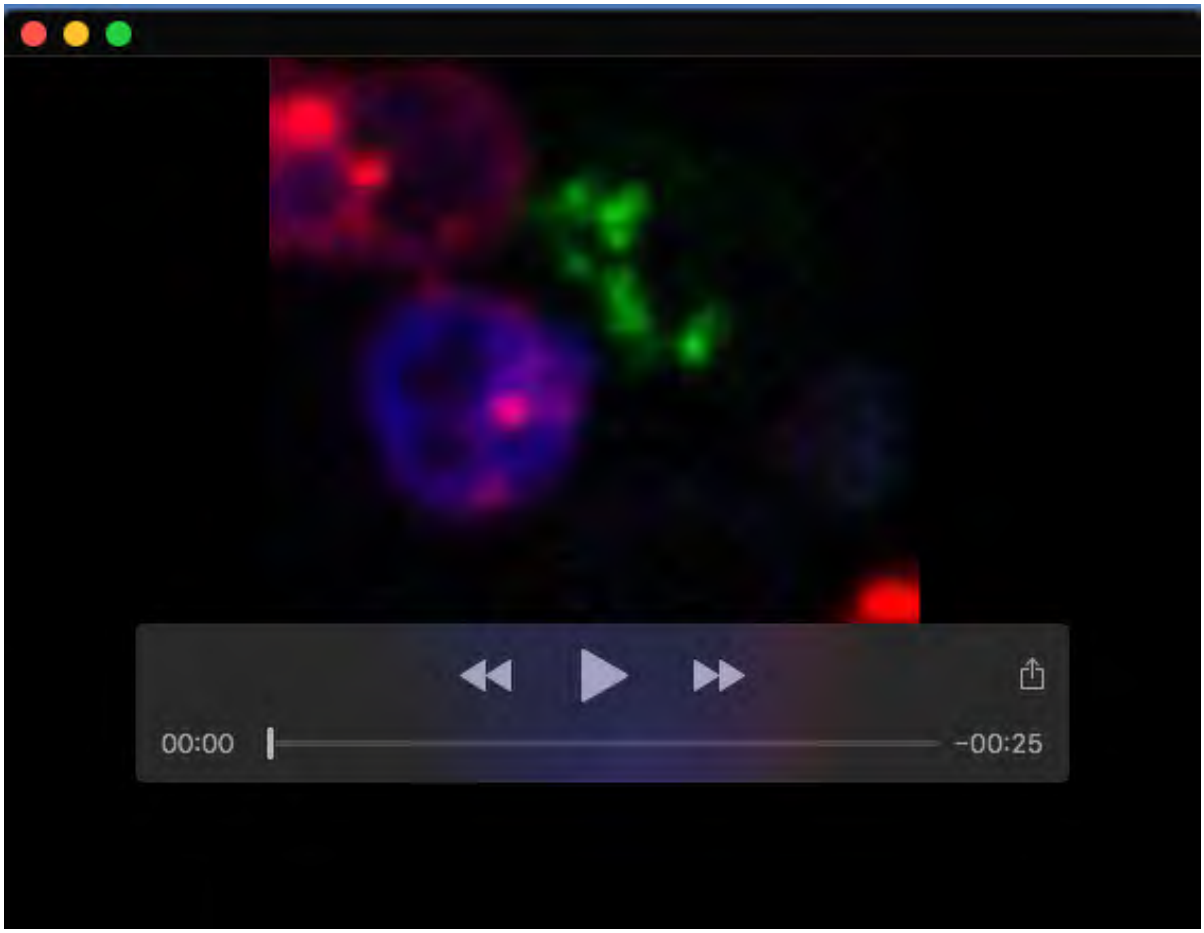

Movie 4. Exchange of Erg6-mCitrine and Dga1-3mCherry in mutants with a delay in ER fusion.

Mating between *sey1 dsl1ΔE* mutant cells expressing Erg6-mCitrine or Dga1-3mCherry and CFP. Note the accumulation of LDs at the fusion neck between the gametes. Expression of the LD marker proteins was repressed 2 h prior to imaging acquisition. Single-plane images were recorded at 1 min intervals.

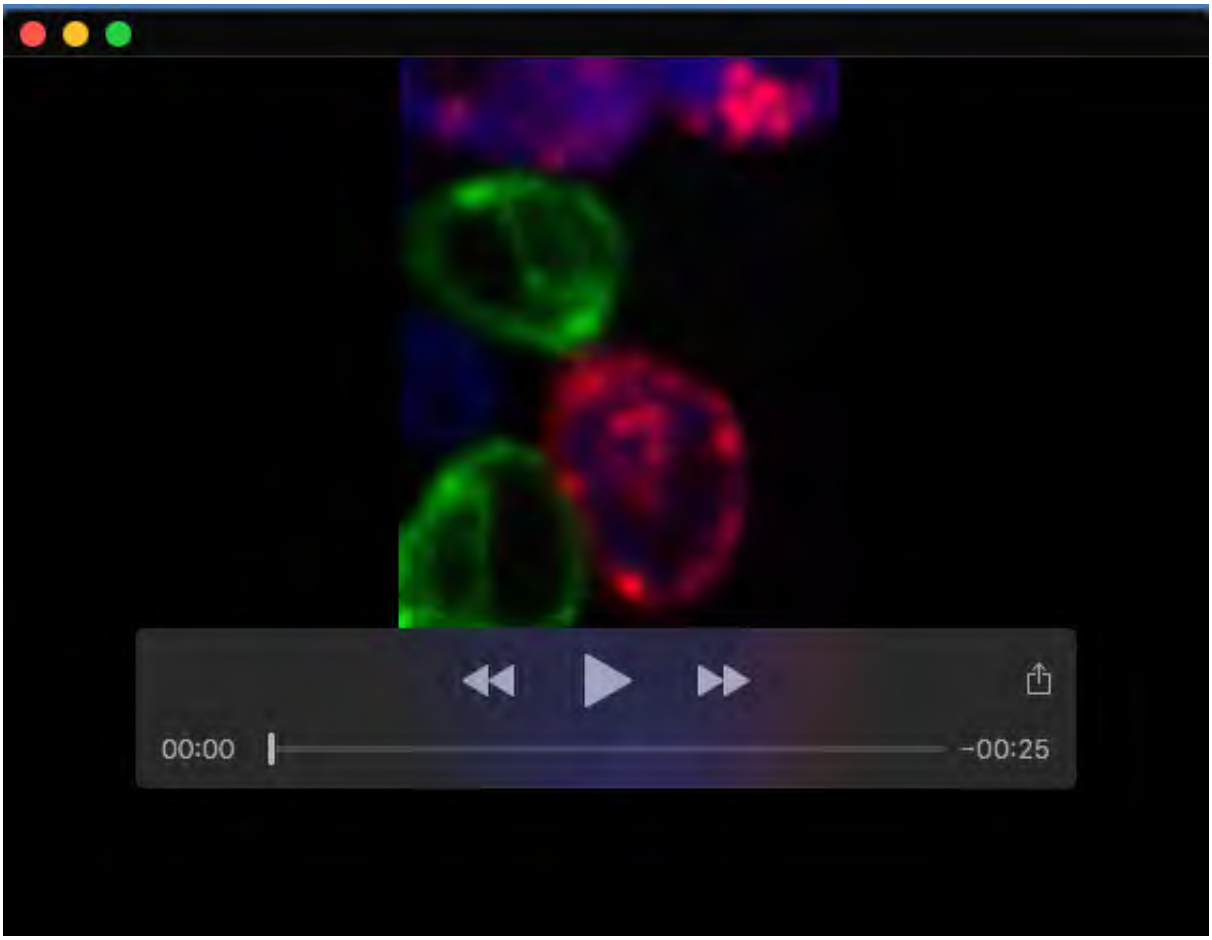

Movie 5. Erg6-mCitrine located in the ER of a quadruple mutant lacking LDs moves to LDs of the mating partner expressing Dga1-3mCherry

Time-lapse images of a *MAT*a cell expressing Dga1-3mCherry and CFP mating with a *MAT*α quadruple mutant 4 (*are1*Δ *are2*Δ *dga1*Δ *lro1*Δ*)* lacking LDs and expressing ER-localized Erg6-mCitrine. Expression of the LD marker proteins was repressed 2 h prior to imaging acquisition. Single-plane images were recorded at 1 min intervals.

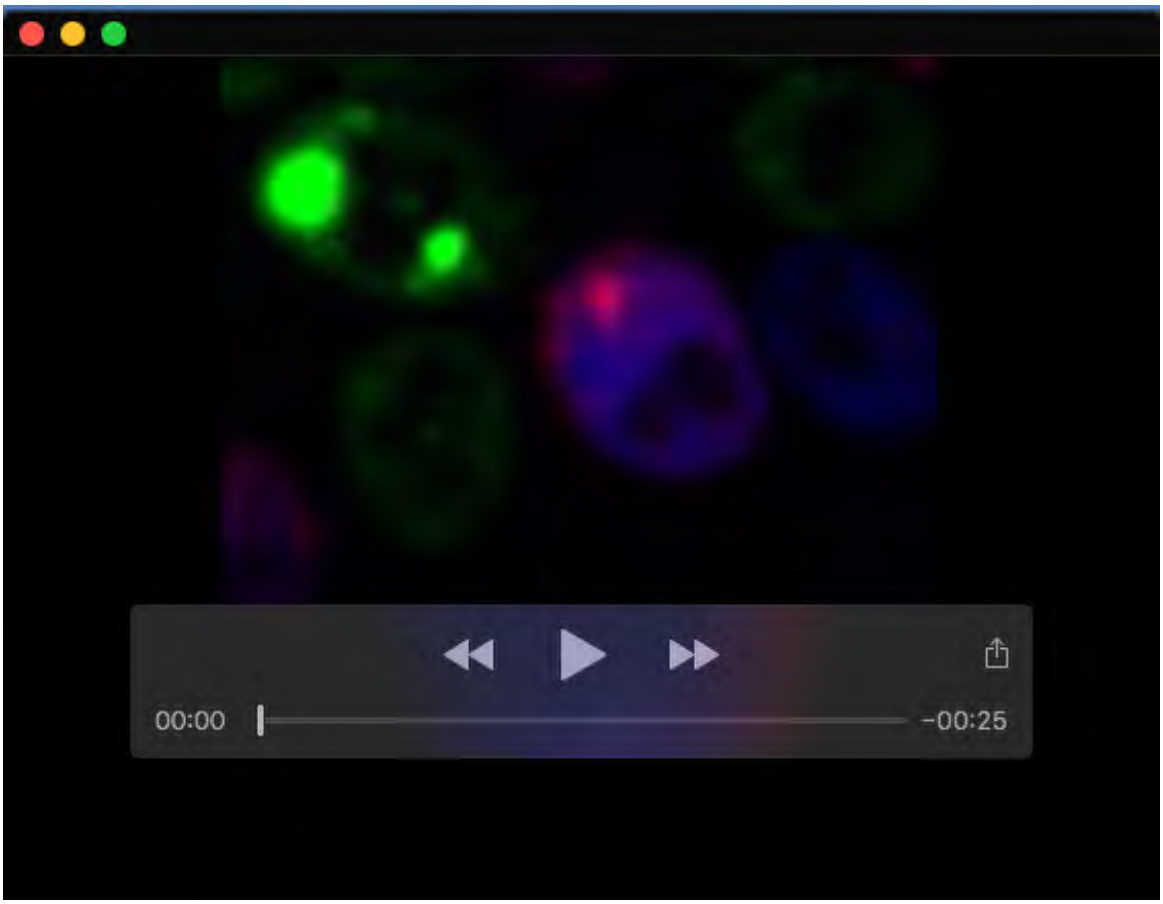

Movie 6. Seipin affects relocalization of LD markers upon zygote formation.
Zygote formation between seipin mutant cells *(fld1Δ)* expressing Dga1-3mCherry and CFP or Erg6-mCitrine. Note the large, possibly clustered LDs in both mating partners, a characteristic of seipin mutants. Expression of the LD marker proteins was repressed 2 h prior to imaging acquisition. Single-plane images were recorded at 1 min intervals.

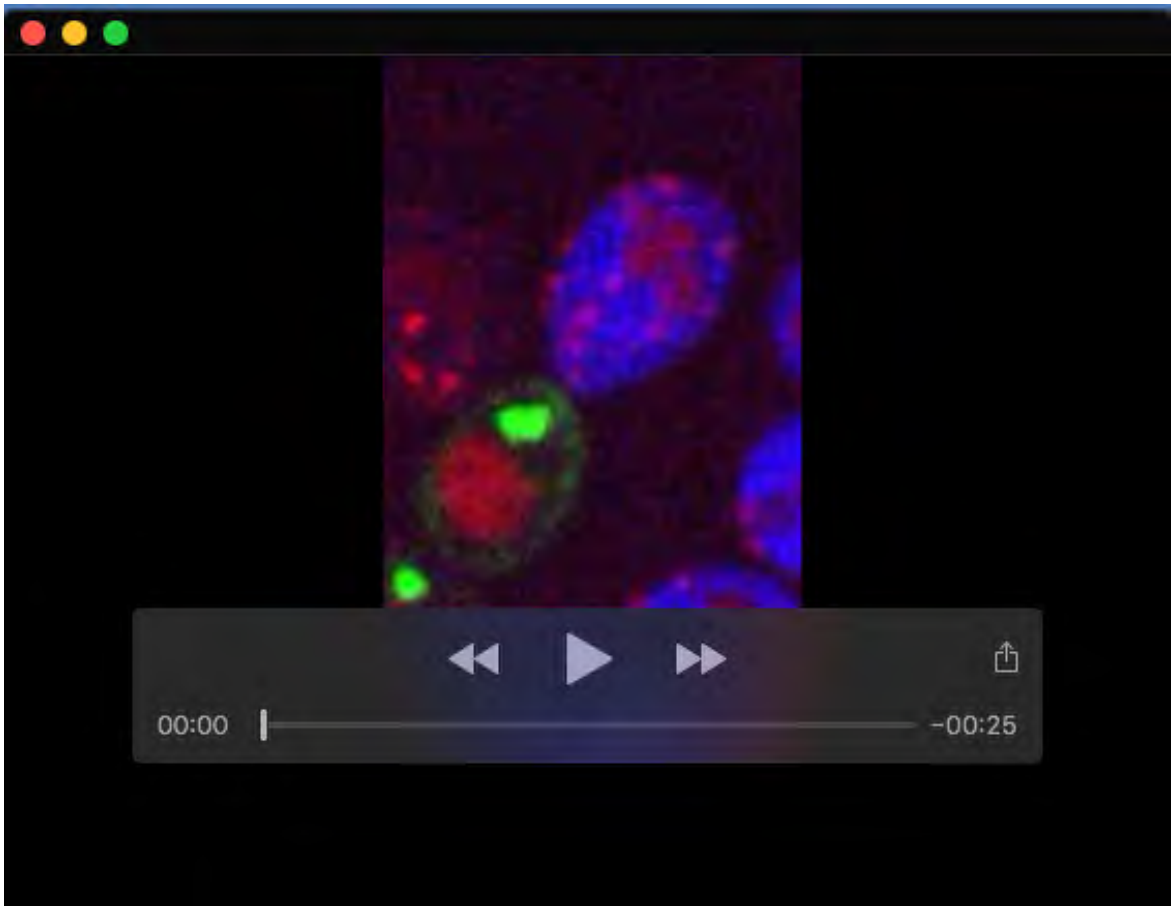

Movie 7. ER sites marked by seipin in wild-type cells acquire the LD marker from the mating partner upon zygote formation.

Mating progression between a cell co-expressing 2mCherry-tagged seipin and CFP and a partner cell expressing Erg6-mCitrine. Erg6-mCitrine expression was repressed 2 h before imaging. Single-plane images were recorded at 2 min intervals.

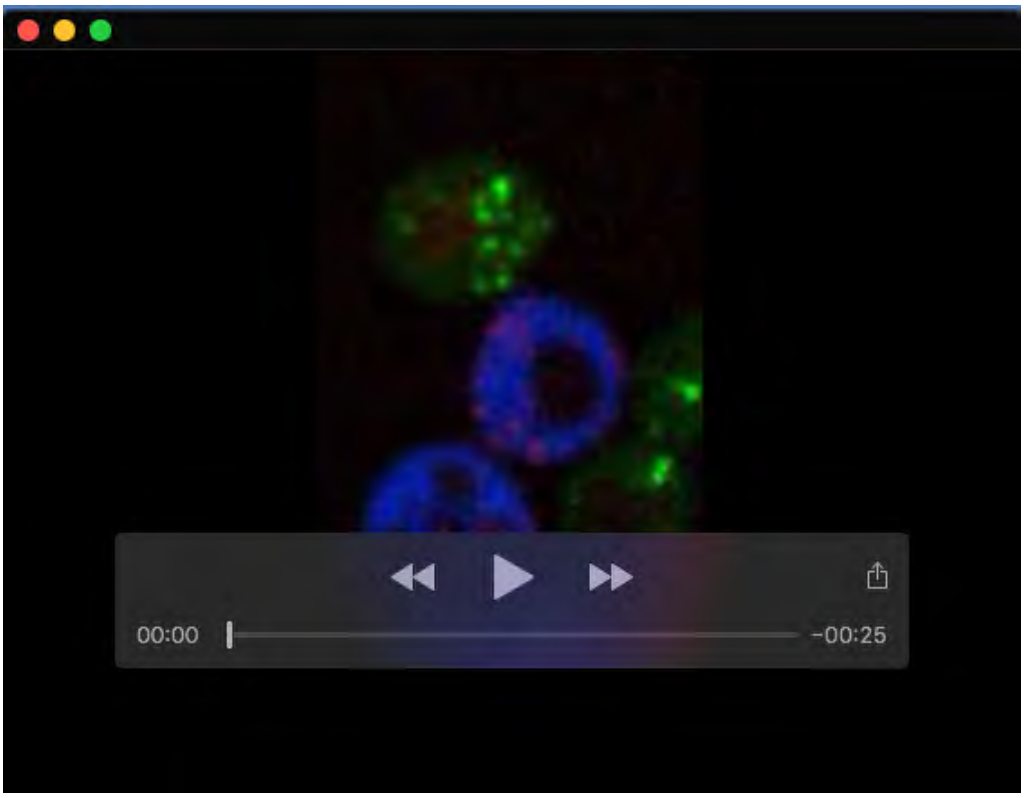

Movie 8. Seipin domains in the ER are stable and do not mix upon zygote formation.

Zygote formation between mating partners expressing red- and green-fluorescently tagged seipin variants. Time-lapse images of a mating between cells of different mating types expressing either Fld1-2mCherry or a split-GFP Fld1-GFP11$_{x7}$ together with BFP and GFP1-10, respectively. Mating progression was followed by acquisition of single plan images separated by 2 min intervals.

Supplementary References

Cottier, S., Darwiche, R., Meyenhofer, F., Debelyy, M. O. and Schneiter, R. (2020). The yeast cell wall protein Pry3 inhibits mating through highly conserved residues within the CAP domain. *Biol Open.* **9,**

Dultz, E. and Ellenberg, J. (2010). Live imaging of single nuclear pores reveals unique assembly kinetics and mechanism in interphase. *J Cell Biol.* **191,** 15-22.

Herskowitz, I. and Jensen, R. E. (1991). Putting the HO gene to work: practical uses for mating-type switching. *Methods Enzymol.* **194,** 132-146.

Jansen, G., Wu, C., Schade, B., Thomas, D. Y. and Whiteway, M. (2005). Drag&Drop cloning in yeast. *Gene.* **344,** 43-51.

Kamiyama, D. et al. (2016). Versatile protein tagging in cells with split fluorescent protein. *Nat Commun.* **7,** 11046.

Mumberg, D., Muller, R. and Funk, M. (1995). Yeast vectors for the controlled expression of heterologous proteins in different genetic backgrounds. *Gene.* **156,** 119-122.

Rogers, J. V., McMahon, C., Baryshnikova, A., Hughson, F. M. and Rose, M. D. (2014). ER-associated retrograde SNAREs and the Dsl1 complex mediate an alternative, Sey1p-independent homotypic ER fusion pathway. *Mol Biol Cell.* **25,** 3401-3412.

Salo, V. T. et al. (2019). Seipin Facilitates Triglyceride Flow to Lipid Droplet and Counteracts Droplet Ripening via Endoplasmic Reticulum Contact. *Dev Cell.*

Sheff, M. A. and Thorn, K. S. (2004). Optimized cassettes for fluorescent protein tagging in Saccharomyces cerevisiae. *Yeast.* **21,** 661-670.

Westermann, B. and Neupert, W. (2000). Mitochondria-targeted green fluorescent proteins: convenient tools for the study of organelle biogenesis in Saccharomyces cerevisiae. *Yeast.* **16,** 1421-1427.